



Electrochemical deposition of metal on diamond  
for applications in thermionic emission and  
electrocatalysis

**SIMON WATSON**  
UNIVERSITY OF BRISTOL  
SCHOOL OF CHEMISTRY

This thesis is submitted in partial fulfilment of the requirements for the Honours  
Degree of MSci at the University of Bristol

Supervisor: Paul May  
Second Assessor: Neil Fox  
Third Assessor: Mike Ashfold  
Physical and Theoretical



## Abstract

The electrochemical phenomenon of underpotential deposition (UPD) has been investigated as a method to controllably deposit a metal monolayer onto a boron-doped diamond (BDD) surface. The purpose of forming a metal monolayer terminated diamond film was to develop an electrocatalyst and a thermionic emitter. Specifically, this thesis analyses the capability of forming a Cu monolayer on hydrogen- and oxygen-terminated BDD films via UPD in 0.1 M H<sub>2</sub>SO<sub>4</sub> + 1 mM CuSO<sub>4</sub>, 2.5 mM CuSO<sub>4</sub> and 2.5 mM CuSO<sub>4</sub> + 0.5 mM KCl solutions.

Cu UPD was observed to a limited extent on hydrogen-terminated BDD films in 0.1 M H<sub>2</sub>SO<sub>4</sub> + 1 mM CuSO<sub>4</sub>, 2.5 mM CuSO<sub>4</sub> and 2.5 mM CuSO<sub>4</sub> + 0.5 mM KCl solutions. The largest coverage of Cu UPD, at ~2 % monolayer coverage, was achieved in the 2.5 mM CuSO<sub>4</sub> solution. The greater quantity of Cu UPD achieved in the 2.5 mM CuSO<sub>4</sub> solution correlated to the more favourable interactions between the diamond surface and Cu<sup>2+</sup> ions. However, oxidation of the hydrogen-terminated BDD electrode prior to the Cu UPD in the 0.1 M H<sub>2</sub>SO<sub>4</sub> + 1 mM CuSO<sub>4</sub> and 2.5 mM CuSO<sub>4</sub> + 0.5 mM KCl solutions was also deemed to have affected the surface quality. As oxygen-terminated surfaces were shown to inhibit the occurrence of UPD, the oxidation of the surface was determined to have a significant role in reducing Cu UPD. The low metal coverage attained using UPD on BDDs was determined to be a limiting factor that currently restricts the use of UPD to synthesise a thermionic emitter or an electrocatalyst modified BDD.

Surface-limited redox replacement (SLRR) depositions were used to replace a Cu UPD ad-layer and bulk deposited Cu (deposited at low overpotentials) with Pt on a BDD film. The Cu deposits were successfully red-ox replaced with Pt in a 0.5 mM K<sub>2</sub>PtCl<sub>4</sub> + 0.1 M HClO<sub>4</sub> solution. However, the low Cu UPD ad-layer coverage limited the Pt coverage that could be achieved. If an epitaxial metal monolayer is attained on a BDD, this research determined that a SLRR deposition is capable of loading a monolayer of a more noble catalytic metal onto the BDD with atomic scale precision.



## **Acknowledgements**

Firstly, I would like to thank Professor Paul May and Dr Natasa Vasiljevic for providing their expertise and guidance throughout this project. Additionally, my thanks go to Mr Michael James and Ms Alicja Szczepanska for their day-to-day assistance and the time they dedicated to helping me.

Finally, I would like to thank all my friends and family for their help, motivation and support while I have been at the University of Bristol - I am truly grateful.



<b>CHAPTER 1: INTRODUCTION</b> .....	<b>9</b>
1.1 UNDERPOTENTIAL DEPOSITION .....	9
1.1.2 <i>Background of Underpotential deposition</i> .....	9
1.1.3 <i>Underpotential Deposition Theory</i> .....	11
1.1.4 <i>Thermodynamics</i> .....	13
1.1.5 <i>Kinetics</i> .....	17
1.1.6 <i>Phase Structure</i> .....	18
1.2 DIAMOND .....	21
1.2.1 <i>Properties of Diamond</i> .....	21
1.2.2 <i>Chemical Vapour Deposition of Diamond</i> .....	24
1.2.2.1 <i>Doping</i> .....	25
1.2.2.2 <i>Surface Terminations</i> .....	26
1.2.2.3 <i>Negative Electron Affinity</i> .....	27
1.3 UNDERPOTENTIAL DEPOSITION APPLIED TO DIAMOND.....	28
1.3.1 <i>Thermionic emission</i> .....	31
1.3.2 <i>Electrocatalysis</i> .....	35
1.4 OBJECTIVES.....	36
<b>CHAPTER 2: EXPERIMENTAL</b> .....	<b>37</b>
2.1 DIAMOND .....	37
2.1.1 <i>Diamond Growth</i> .....	37
2.1.2 <i>Electrochemical Grade Diamonds</i> .....	37
2.2 TERMINATION TECHNIQUES.....	38
2.2.1 <i>Hydrogen plasma termination</i> .....	38
2.2.2 <i>Oxygen plasma termination</i> .....	38
2.2.3 <i>Ozone exposure in UV</i> .....	39
2.3 ELECTROCHEMICAL EXPERIMENTS.....	39
2.3.1 <i>Copper Underpotential deposition</i> .....	39
2.3.2 <i>Surface-limited redox replacement (SLRR) deposition of Pt</i> .....	40
<b>CHAPTER 3: RESULTS AND DISCUSSION</b> .....	<b>41</b>
3.1 CHARACTERISATION OF DIAMOND FILMS .....	41
3.1.1 <i>HFCVD Diamond Films</i> .....	41
3.1.2 <i>Electrochemical Grade Diamond Films</i> .....	43
3.2 CU UNDERPOTENTIAL DEPOSITION .....	44
3.2.1 <i>Hydrogen-terminated Diamond Films</i> .....	44
3.2.1.1 <i>Solution: 0.1 M H<sub>2</sub>SO<sub>4</sub> + 1 mM CuSO<sub>4</sub></i> .....	44
3.2.1.2 <i>Solution: 2.5 mM CuSO<sub>4</sub></i> .....	49

3.2.1.3 Solution: 2.5 mM CuSO <sub>4</sub> + 0.5 mM KCl.....	52
3.2.1.4 X-ray Photoelectron Spectroscopy (XPS).....	55
3.2.2 <i>Oxygen-terminated Diamond Films</i> .....	57
3.3 SURFACE-LIMITED REDOX REPLACEMENT (SLRR) DEPOSITIONS .....	59
<b>CHAPTER 4: CONCLUSIONS.....</b>	<b>67</b>
<b>CHAPTER 5: FUTURE WORK.....</b>	<b>69</b>
<b>CHAPTER 6: REFERENCES .....</b>	<b>70</b>
<b>CHAPTER 7: APPENDIX.....</b>	<b>76</b>

## Chapter 1: Introduction

### 1.1 Underpotential deposition

#### 1.1.2 Background of Underpotential deposition

Electrochemical deposition of metals has been a widely studied subject over the past century and the scientific understanding of the processes involved has significantly progressed. In the information age, electrochemical deposition techniques cemented their applicability to modern technology as inexpensive and fast methods to deposit metals in the electronics industry [1].

Epitaxial monolayer coverage corresponds to a single layer of atoms or molecules adsorbed on a surface at the maximum surface concentration achievable. It was discovered that when metal monolayers were deposited, different electronic and structural properties of these layers were exhibited in comparison to their bulk deposits. These unique properties of metal monolayers produce distinctive characteristics that enable and enhance a variety of applications, from the microminiaturisation of electronics to electrocatalysis, including enhancing the durability and efficiency of catalysed fuel cells [2, 3]. Various techniques have been developed to form monolayers and ultra-thin films, such as evaporation and sputtering deposition techniques. However, these techniques require expensive ultra-high vacuum (UHV) systems and are not sensitive to monolayer formation. Additionally, issues of alloying have also been shown to intervene and obstruct the formation of a monolayer on metal surfaces.

Underpotential deposition (UPD) is an electrochemical phenomenon that involves the formation of a metal ad-layer on the surface of a foreign substrate by reducing metal ions at potentials more positive than the Nernst equilibrium [4, 5, 6]. In 1935, Haissinsky first indicated that deposition could occur at an 'under-voltage' from studies on the electrochemical deposition of bismuth and polonium on gold and silver electrodes [7]. Kolb, Przasnyski and Gerischer suggested the original theory of UPD in 1974, which attributed the favourability of the monolayer adsorption on the substrate to an ionic

contribution in the chemical bonds from partial electron transfers [8]. Since then, processes have been discovered in many metal-substrate systems and understanding of the phenomenon has developed. Nowadays, the stability of the metal ad-layer is ascribed to the greater binding energy between the substrate and the metal deposit compared to the binding energy between the metal atoms deposited on the same metal.

UPD has been shown in numerous metal adsorbate-bulk metal substrate systems involving polycrystalline and monocrystalline substrates, including Pb/Au(111), Cu/Au(111), Ag/Pt(100), and Tl/Ag(100) [9]. Each system has a different ordered adsorption process, resulting in drastically different phase structures. Cyclic voltammograms that display multiple peaks are used as indicators that ordered adsorption has occurred in a system [10]. These peaks are shown in the UPD region and can be correlated to their associated adsorption structures by various analytical techniques, such as scanning tunnelling microscopy (STM), X-ray diffraction (XRD), and atomic force microscopy (AFM).

Surface-limited reactions of UPD layers have been successfully exploited for a variety of applications. In electrocatalysis, the surface-limited nature of UPD is used to create Pt-bimetallic catalysts [12]. Moreover, underpotentially deposited metal monolayers are exploited in the so-called surface-limited redox replacement (SLRR) depositions. The SLRR process is based on the red-ox replacement of an underpotentially pre-deposited 'sacrificial layer' with an alternative more noble metal than the UPD metal [11]. The result of a single SLRR deposition cycle is the production of an epitaxial monolayer that cannot be achieved by other conventional deposition methods. The atomic precision attained in a SLRR deposition has been used to deposit alternate atomic layers of compound semiconductors [13, 14, 15].

This thesis aims to analyse the capability of using UPD and SLRR depositions to controllably deposit a metal monolayer on a diamond film for applications in thermionic emissions (See Section 1.3.1) and electrocatalysis (See Section 1.3.2).

### 1.1.3 Underpotential Deposition Theory

The UPD phenomenon, which involves the reduction of metal ions onto a foreign substrate (Equation 1) at potentials more positive than the Nernst equilibrium potential, appears to disobey the thermodynamics predictions. The rationale arising from the Nernst equation (Equation 2) is that metals should deposit onto a foreign substrate at potentials lower than the Nernst equilibrium potential [4]. This rationalisation suggests that UPD contradicts the Nernst thermodynamic law of equilibrium for the metal/metal ion system.

The equilibrium reaction between the electrodeposited metal ( $M$ ) and the metal ions in solution ( $M_{(aq)}^{z+}$ ) is given in Equation 1. The Nernst equation for the bulk metal under equilibrium conditions is shown in Equation 2 [5].



$$E_{M/M_{(aq)}^{z+}} = E_{M/M_{(aq)}^{z+}}^0 + \frac{RT}{zF} \ln\left(\frac{a_{M_{(aq)}^{z+}}}{a_M}\right) \quad (2)$$

$E_{M/M_{(aq)}^{z+}}$  is the Nernst equilibrium potential for the bulk metal deposit and the metal ions,  $E_{M/M_{(aq)}^{z+}}^0$  is the standard equilibrium potential for the reaction,  $a_{M_{(aq)}^{z+}}$  and  $a_M$  are activities of the metal ions and the bulk metal deposited, respectively, with  $a_M$  defined as 1,  $T$  is temperature, and  $R$  and  $F$  are the gas and Faraday constants, respectively.

The Nernst equilibrium for the bulk metal represents the potential at which the rate of metal deposition onto the surface equals the rate of dissolution of the deposited metal. Bulk deposition occurs when the electrochemical system is supersaturated with metal ions at potentials smaller than the Nernst equilibrium (the overpotential deposition region). Conversely, the equation predicts the dissolution of the metal adatoms on the substrate in undersaturated systems at potentials greater than Nernst equilibrium.

UPD can be treated as a surface-limited metal adsorption process because it is a two-dimensional process that continues only until all the available surface sites on the

substrate are occupied [5, 16]. Treatment of the metal adatoms ( $M_\theta$ ) adsorbed onto a substrate ( $S$ ) at a certain surface coverage according to the UPD phenomenon in a quasi-Nernst equation is shown in Equation 3 [5].

$$E_{(M_\theta/S)/M_{(aq)}^{z+}} = E_{(M_\theta/S)/M_{(aq)}^{z+}}^0 + \frac{RT}{zF} \ln\left(\frac{a_{M_{(aq)}^{z+}}}{a_{M_{(M_\theta/S)}}}\right) \quad (3)$$

$E_{(M_\theta/S)/M_{(aq)}^{z+}}$  is the equilibrium potential for the metal adatoms adsorbed at the fractional coverage  $\theta$  and the metal ions,  $E_{(M_\theta/S)/M_{(aq)}^{z+}}^0$  is the standard equilibrium potential for the reaction,  $a_{M_{(aq)}^{z+}}$  is the activity of the metal ions, and  $a_{M_{(M_\theta/S)}}$  is the activity of the metal adatoms adsorbed at the fractional coverage  $\theta$ .

An adsorption isotherm (coverage-potential curve) is used to best describe the activity of the adsorbed species at specific coverages and the multiple energy states in a monolayer [4, 17]. Subsequently, the adatoms adsorbed onto the substrate to form sub-monolayers and monolayers have an activity less than the activity of a bulk metal deposit (which is equal to 1) [5]. The smaller activity of a metal sub-monolayer and monolayer shifts the equilibrium for UPD to a more positive potential than calculated by the Nernst equation (Figure 1).

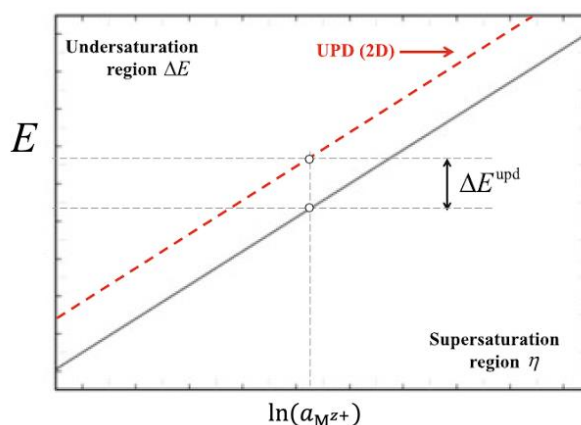


Figure 1: Illustration of the UPD potential shift as the difference between the equilibrium potential for two-dimensional UPD ad-layer (red dotted line) and the Nernst equilibrium for the reaction (black line). Image taken from reference [5].

The difference between the equilibrium potential for monolayer quantities of metal to be deposited on a foreign substrate and the Nernst equilibrium potential for a system has been denoted as the UPD potential shift, represented by  $\Delta E^{\text{UPD}}$  in Figure 1 [4]. The UPD potential shift indicates that stable two-dimensional phases of metal adatoms are feasible at potentials more positive than the Nernst equilibrium from the Nernstian considerations.

#### 1.1.4 Thermodynamics

The ability for UPD to occur is primarily attributed to the greater binding energy achieved for adsorbing a metal adatom onto the surface of a foreign substrate ( $M$ - $S$ ) relative to the deposition of a metal atom on a surface of the same metal ( $M$ - $M$ ) [4, 18, 19]. The stronger attraction between the substrate and the metal adatoms makes the adsorption of metal onto the substrate more favourable than bulk depositing the metal [20]. Thus, the favourable UPD electrodeposition on the substrate surface constructs a two-dimensional phase rather than a bulk deposit. Consequently, UPD phases are generally limited to an epitaxial monolayer and is why UPD can be considered as a surface adsorption-like process.

In earlier studies, the UPD potential shifts,  $\Delta E^{UPD}(\Theta)$ , were initially correlated to the differences in work functions of the substrate and the metal ad-layer deposit,  $\Delta\Phi$ , shown in Equation 4 [8].

$$\Delta E^{UPD}(\Theta) = 0.5 \Delta\Phi \quad (4)$$

However, the correlation was shown not to be universal for all UPD systems because the process is particularly sensitive to the crystal orientation of the substrate [22]. Generally, different single-crystal surface faces, for example (111) and (100), in the same metal-substrate system have different UPD potential shifts, even though the same difference in work function is exhibited. Nevertheless, the difference in work function does have a notable importance in determining the magnitude of the UPD shift and thus the stability of the monolayer.

Kolb *et al.* and Schmickler subsequently derived the concept of the UPD potential shift from different perspectives [6]. Kolb *et al.* equated the chemical potentials for the reduction of metal ions onto the same metal to the reduction of metal ions onto a substrate. This attained a general UPD expression for the surface coverage of adatoms on a substrate. Schmickler's derivation produced an analogous equation in terms of the binding free energy of a metal deposited onto a substrate and the binding free energy of a metal deposited onto an atom of the same kind [21].

Formation of a metal monolayer utilising the UPD phenomenon involves several different processes (Figure 2). The solvated metal ions in the electrolyte move to the reaction zone at the electrode surface. At the reaction zone, the electron transfers are facilitated, which consequently leads to the adsorption of adatoms [23]. The accumulation of different charges between the solid electrode and the electrolyte causes a potential difference at the interface and thus the electrochemical double-layer formation. The inner Helmholtz plane (IHP) of the electrochemical double-layer is the distance from the electrode surface where species are adsorbed onto the electrode and corresponds to the

reaction zone regarding the UPD phenomenon. The outer Helmholtz plane (OHP) of the double-layer represents the plane of closest approach of solvated ions. In UPD, work is done to move the metal ions from the OHP to the IHP. The work done instigates the loss of the solvation shell surrounding the metal ions and displaces solvent on the electrode surface to allow the chemisorption process to occur [24].

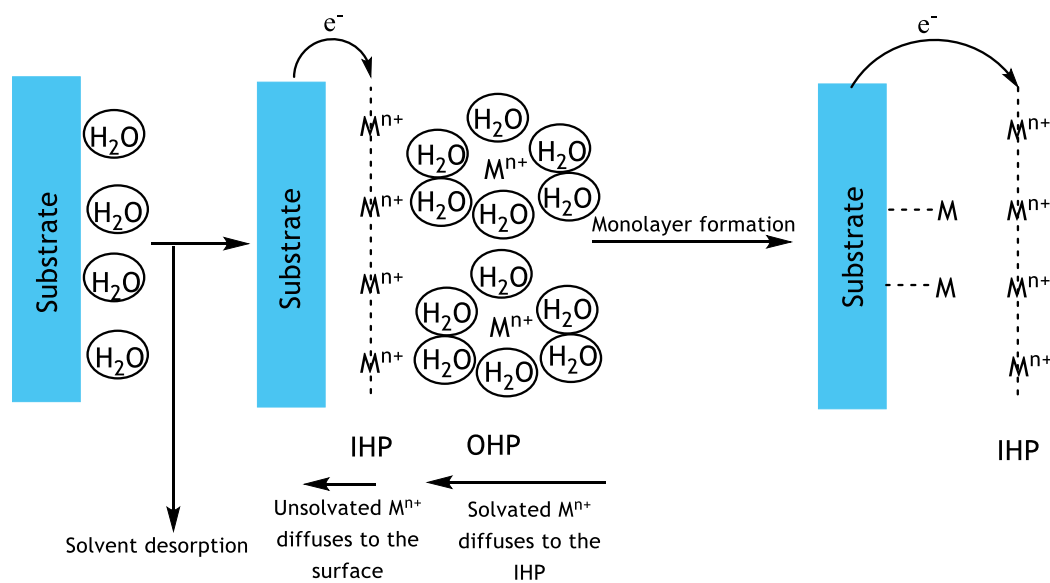


Figure 2: Representation of the adsorption process of metals onto a substrate in the underpotential deposition phenomenon. Image adapted from reference [23].

The electrons are transferred at the electrode surface causing a partial or full reduction of the metal ions. The partial electron transfer in the chemisorption process can be considered as a thermodynamic property of electro-sorption valency and leads to the co-adsorption of anionic species in the electrolyte [25]. The favourability of the electron transfer process to the metal ions is dependent on the work function of the substrate as a determining factor on the ability to release electrons [23]. The energy of the electron transfer, atomic rearrangement and the work done moving the metal ions to the reaction zone, including the desolvations, must be overcompensated by the substrate-metal

bonding interaction to enable the metal to be deposited as an adatom and prompt monolayer formation.

Different isotherm models can describe the adsorption of metals in UPD systems. These adsorption isotherms account for different types of interactions between ions and substrate. The Langmuir adsorption isotherm assumes that all the adsorption sites are equivalent, independent of the presence of surrounding adatoms and that maximum adsorption is limited to a monolayer [26]. Thus, the Langmuir adsorption isotherm has greater applicability to UPD systems at a low coverage, generally below  $\theta = 0.2$ , because it is more viable to neglect the surrounding interactions [4]. At increased monolayer coverage, adsorption sites are not all energetically identical and different adsorption energies are associated with different sites. The Temkin isotherm model accounts for changes in surface coverage, assuming the free energy of the monolayer decreases linearly with coverage [4]. Additionally, lateral particle-particle interactions contribute to variations in the monolayer free energy. Depending on the charge transferred, the lateral interactions in UPD systems are either between fully discharged metal atoms or partially discharged metal ions. The partially discharged systems result in repulsion between the adsorbed species, which is relieved to a certain degree by the co-adsorption of the anionic species in the electrolyte. The lateral interactions were resolved in different adsorption isotherms for different approximations by Honig, Frumkin, and Fowler and Guggenheim to provide better correlations at higher monolayer coverages [27].

Experimental investigations are used to determine the most appropriate adsorption isotherm to describe a system. The adsorption isotherms that best fit the experimental data provide information on the phase transitions that occur and the activity of the metal adatoms adsorbed at certain fractional coverages in particular systems.

### 1.1.5 Kinetics

The significant kinetic aspects involved in the UPD phenomenon are the bulk diffusion of the solvated metal ions, charge transfer from the substrate, surface diffusion of the metal adatoms, and the first- or high-order phase transitions [27]. The kinetic controls for UPD systems can depend on the potential applied at the electrode and lead to mixed controlled systems, for instance, favouring charge transfer control at more positive potentials and mass-transport control at more negative potentials [17].

UPD systems are generally deposited in dilute solutions, giving the bulk diffusion processes greater significance in the kinetic control of the monolayer formation [4]. In mass-transport controlled processes, the ions are immediately adsorbed upon reaching an available site on the substrate surface regardless of the adsorption energy. The adatoms deposited in the less favourable sites would eventually migrate in a surface diffusion process to the more energetically stable positions on the substrate. Thus, the electrode surface is modified by the chemisorption of metals, which changes the double-layer capacitance and initiates double-layer effects that interfere with the mass flux data to the electrode in UPD systems [28]. Rotating ring-disk electrodes (RRDE) and thin-layer techniques have been widely exploited in UPD studies to distinguish between current and mass flux data in determining the kinetics at the electrode [28].

The inhomogeneous substrate surface approach was developed to describe the kinetics of UPD systems that accounts for the surface inhomogeneities and surface diffusion in systems, which are not controlled by bulk diffusion [27, 29]. In this approach, the charge transfer at discontinuities is differentiated from the less favourable charge transfers at the terraces and includes the surface diffusion of the adatoms. The model accounts for the differing charge transfer resistance on the inhomogeneous substrate surface. However, the model neglects the bulk diffusion of the solvated metal ions and lower dimensional adsorbed phases affecting the electrode [29].

### 1.1.6 Phase Structure

UPD processes are sensitive to the crystallographic orientation of the substrate. Different substrate crystallographic orientations can considerably affect the UPD shift and the type of structural phases that are deposited.

UPD processes generally start at the substrate defect sites. Crystal defects - steps, kinks and vacancies - provide additional substrate metal bonding sites and a more energetically favourable site for the metal to deposit [30]. The defects in the substrate surface subsequently act as growth sites for the formation of the monolayer and significantly influence the initial steps of 2-D monolayer electrodeposition.

The 2-D metal adatom structural arrangement varies according to different aspects regarding the substrate and the metal. The metal monolayer is classified from the crystallographic misfit with respect to the substrate either as commensurate, higher order commensurate or incommensurate (Figure 3) [29]. Generally, the phase structure formation initially proceeds via an expanded commensurate or random ad-layer structure on the substrate terraces. First-order phase transitions occur at an increased surface concentration and drive the formation of the 2-D metal monolayers [27, 31]. Commensurate arrangements (Figure 3a and 3b) are the result of translational symmetry of the monolayer-substrate lattice enabling the adsorbed metal atoms to occupy the most favourable adsorption sites [32]. Either higher-order commensurate (Figure 3c) or incommensurate (Figure 3d) arrangements form when there is significant lattice misfit between the substrate and the metal ad-lattice. The arrangement formed is determined by the most energetically stabilising structure. Higher-order commensurate structures involve a compressed ad-lattice with occasional adatoms occupying the most favourable adsorption sites. Conversely, adatoms in the incommensurate arrangements are unable to occupy the most favourable adsorption sites.

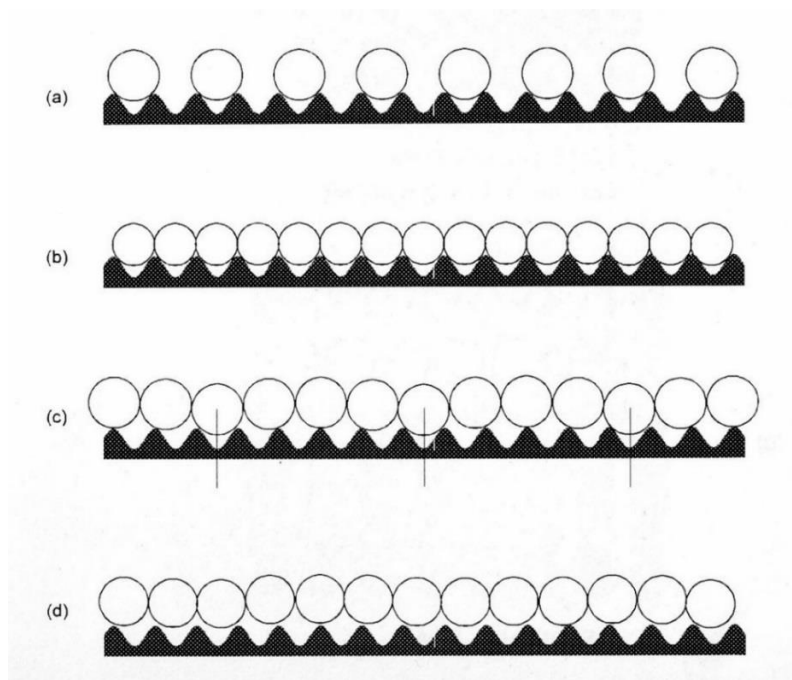


Figure 3: Representation of the metal ad-layer crystallographic misfits with respect to a single-crystal substrate; (a) and (b) are commensurate ad-layers, (c) is a higher order commensurate ad-layer, and (d) is an incommensurate ad-layer. Image taken from reference [27].

Stabilised UPD ad-layers can show vastly different surface structures and interfacial properties compared to the bulk metal. The three well established Cu phases that form on Au(111) in a sulfate solution (Figure 4) show the array of surface structures that can be observed in a system [33]. The lattice spacing in bulk Cu is much smaller than that of Au, which means the Cu UPD ( $1 \times 1$ ) monolayer formed on Au(111) is particularly strained from stretching [34]. The strained metal monolayer phase and the distinct  $(\sqrt{3} \times \sqrt{3}) R30^\circ$  honeycomb superstructure exemplify the broad range of structural arrangements that can be formed by UPD in comparison to the bulk metal deposits. The differing ad-layer arrangements formed by UPD systems affect the electronic properties, altering the properties relative to the bulk deposit. These tuneable features of the UPD metal monolayers provide significant opportunities in electrocatalysis applications (See Section 1.3.2).

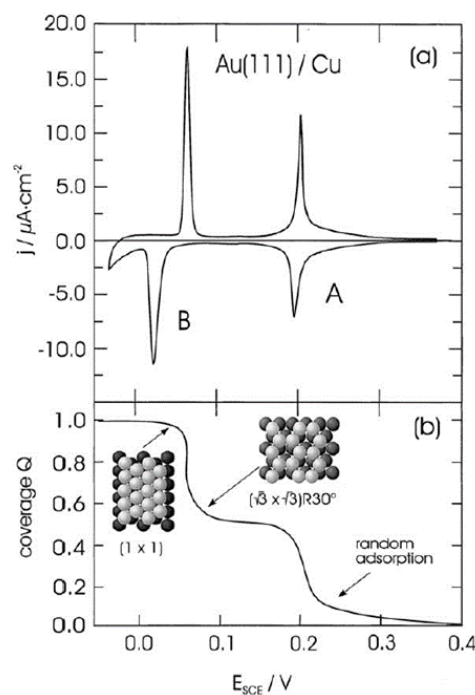


Figure 4: (a) Cyclic current density-potential voltammogram and (b) adsorption isotherm  $\theta(E)$  for the Cu (light-grey spheres) monolayer formation on Au(111) (black spheres) in a 0.05 M  $H_2SO_4$  + 1 mM  $CuSO_4$  solution at a scan rate of  $1 \text{ mV s}^{-1}$ . Image taken from reference [33].

In UPD, the anionic species in the electrolyte are also a vital component. The anionic species have the ability to considerably alter the structure of UPD ad-layers [35]. Diverse structures observed in some UPD ad-layers are attributed to the repulsive forces associated with the co-adsorbed anions or partial charges on the metal adatoms [36]. The stabilising capacity that co-adsorbed anionic species provide to monolayer structures that are expected to be unstable is most notably demonstrated by the  $(\sqrt{3} \times \sqrt{3}) R30^\circ$  honeycomb Cu ad-layer on an Au(111) in sulfate solution (Figure 5) [37]. Consequently, the substrate and the electrolyte solution both considerably influence the UPD phases that are formed in a system.

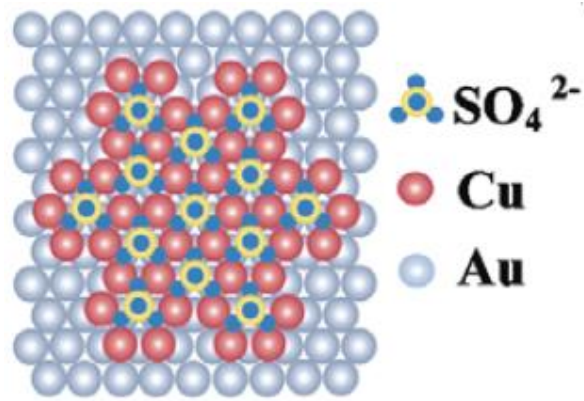


Figure 5: Illustration of the  $(\sqrt{3} \times \sqrt{3}) R30^\circ$  honeycomb superstructure in Cu UPD on Au(111) in a sulfate solution. Image taken from reference [34].

## 1.2 Diamond

### 1.2.1 Properties of Diamond

Diamond has been distinguished from other materials for a variety of purposes. It possesses the highest thermal conductivity at room temperature and is one of the hardest, stiffest, and least compressible known materials [38]. Therefore, numerous industries have aimed to utilise diamonds and exploit these exceptional physical properties. The high cost of diamonds and the inability to attain natural diamonds in a desired structure are the limiting factors that initially hindered the ability to widely harness these specialist properties, some of which are shown in Table 1 [39]. Despite these factors, natural diamond applications were established in certain industries for abrasive purposes, utilising the poor-quality stones, whereas the premium-quality costly diamonds have been widely reserved for use as gemstones for the ornamentation of extravagant items [39, 40].

Table 1: Some impressive properties that diamond possess. Image adapted from reference [41].

Property	Value	Units
Hardness	$1.0 \times 10^4$	kg mm <sup>-2</sup>
Strength, tensile	> 1.2	GPa
Strength, compressive	> 110	GPa
Density	3.52	g cm <sup>-3</sup>
Young's modulus	1.22	GPa
Thermal conductivity	20.0	W cm <sup>-1</sup> K <sup>-1</sup>
Dielectric constant	5.7	Dimensionless
Work function	Negative	On [111] surface
Bandgap	5.45	eV
Resistivity	$10^{13}$ - $10^{16}$	$\Omega$ cm

After combustion experiments on diamond in the late 1700s, chemists determined that diamond consisted of carbon only and thus was an allotrope of graphite [42]. Diamond is comprised of tetrahedral  $sp^3$  hybridised carbons in a face-centred cubic crystal structure (Figure 6) and is the metastable carbon allotrope at room temperature [43]. The strong  $\sigma$ -bonds and dense packing of the carbon atoms in a three-dimensional tetrahedral network (Figure 6) are responsible for inducing the impressive array of physical properties. The thermodynamically stable graphite allotrope consists of stacked  $sp^2$  hybridised carbon hexagonal layers with weak van der Waals bonding interactions, due to the delocalised  $\pi$ -system between the adjacent layers. These significantly different structures consequently cause very different properties to be exhibited, even though both structures are made up solely of elemental carbon [44]. A large phase transition activation barrier separates the two allotropes and contributes to the rarity and kinetic stability of diamonds on the Earth's surface.

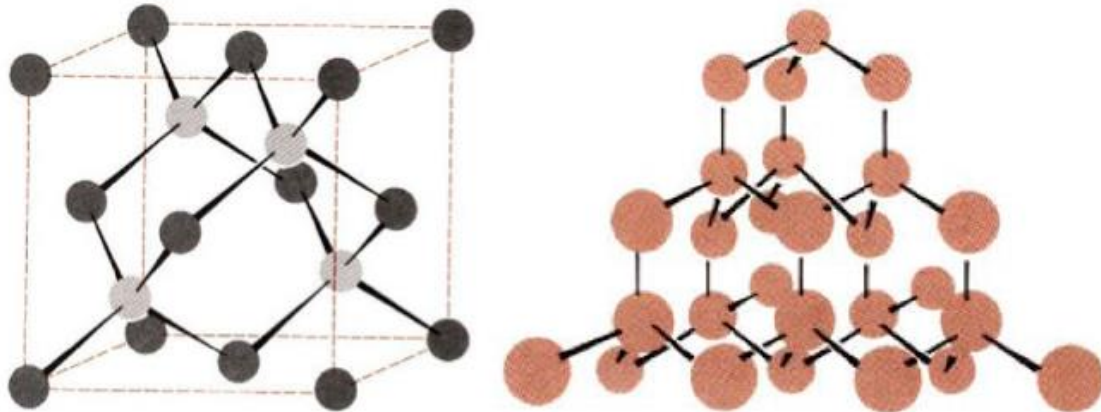


Figure 6: A representation of a diamond unit cell with the face-centred cubic crystal structure positions indicated in dark grey (left) and the three-dimensional diamond tetrahedral network (right) - each sphere corresponds to a carbon atom. Image taken from reference [43].

The demand for diamonds has increased globally and is in disjuncture with the current excavation rate of natural diamond. This limits the sustainability of the natural diamond industry. In 1955, the ambitious process to replicate the synthesis of diamonds under high pressure-high temperature (HPHT) conditions in a laboratory was attempted and determined that the process could not reproduce diamonds at grades similar to those produced naturally [45]. Nevertheless, due to their lower cost relative to natural diamonds, small diamond grains synthesised from the HPHT conditions have been able to act as a substitute for the lower quality natural diamonds used in industry; it is estimated that synthetic diamonds now account for 90 % of the diamonds used in industry [39].

### 1.2.2 Chemical Vapour Deposition of Diamond

Rather than replicating the HPTP conditions in nature, alternative metastable growth of diamond at low pressures was postulated from precursors with high chemical potentials [45]. The diamond phase that forms under these specific conditions are unable to convert from the metastable configuration to the thermodynamically stable graphite phase because the energy to surpass the phase transition activation barrier is unattainable. With this understanding, Eversole first synthesised diamond in a chemical vapour deposition (CVD) process from a carbon-containing gas [46]. Eversole's experimental work prompted groups to further this research, which subsequently led to the development of the hot filament (HF) and microwave plasma CVD reactors in 1982 and 1983 respectively [47, 48].

The initial investigations found that the diamonds synthesised in the CVD had a mixture of diamond and graphite phases. Angus *et al.* discovered that including atomic hydrogen was the critical element required to develop high quality CVD diamond films [49]. The inclusion of hydrogen was the crucial piece of the puzzle for removing the graphite impurities in the CVD diamond syntheses. This is because of the hydrogen etching rate, which in certain conditions exceeds the graphite growth rate but not the diamond growth rate [50]. Furthermore, the hydrogen is also considered as a vital component in other processes in CVD growth: termination of the dangling bonds on the diamond surface, driving faster diamond growth rates by reacting with the neutral carbon-containing gases, and preventing the accumulation of long-chained hydrocarbons [38]. The importance of atomic hydrogen is reflected in the gas mixing ratio for typical CVD diamond syntheses of 1 % vol. CH<sub>4</sub> diluted in hydrogen.

Homoepitaxial and heteroepitaxial diamond nucleation have been established in literature [51]. The homoepitaxial method requires a diamond substrate to provide nucleation sites. The diamond substrate enables carbon addition to expand on the existing diamond tetrahedral lattice. Heteroepitaxial growth on non-diamond substrates cannot provide a diamond tetrahedral lattice for additional carbons to extend. Non-diamond substrates are

required to form a carbide interfacial layer that stabilises the diamond nucleation. The carbide interfacial layer reduces the lattice mismatch between the substrate and diamond at the interface. Substrates are only feasible to use if the material's melting point is above the reactor operation temperature, have a thermal expansion coefficient similar to that of diamond, and are able to form an appropriately thick carbide layer [38]. Si wafer is one example of a commonly used substrate in CVD diamond synthesis.

### 1.2.2.1 Doping

Undoped diamond has a wide-bandgap (5.45 eV) that restricts the flow of electrons into the conduction band, making diamond an electrical insulator. However, incorporating certain impurities, known as doping, can alter the electrical conductivity of CVD diamond films to make diamond a semiconductor. *N*-type doping requires donor atoms to have an excess of valence electrons with respect to carbon, such as nitrogen or phosphorus. By contrast, *p*-type doping requires acceptor atoms with one less valence electron than carbon, like boron, to be introduced into the diamond lattice.

The excess electrons in *n*-type doping fill a new donor energy level in the band gap. As the electrons can be excited into the conduction band from the donor energy level, less energy is required to promote the electrons into the conduction band (Figure 7). Nitrogen-doped diamond produces a deep donor energy level and therefore only provides a relatively small decrease in the energy gap to the conduction band (to 4 eV). However, thermal vibrations broaden the donor energy level for nitrogen-doped diamond, which consequently causes a further decrease in the energy gap to reach the conduction band (Figure 7) [52]. In *p*-type doping, an acceptor energy level above the valence band maximum in the band gap is generated and can accept excited electrons (Figure 7). The electrons promoted to the acceptor energy level produces electron holes in the valence band, which enables the electrons in the valence band to move and the material to become conductive. The boron-doped diamond (BDD) acceptor energy level is generally

situated 0.4 eV above the valence band maximum and subsequently can be considered as a semiconductor.

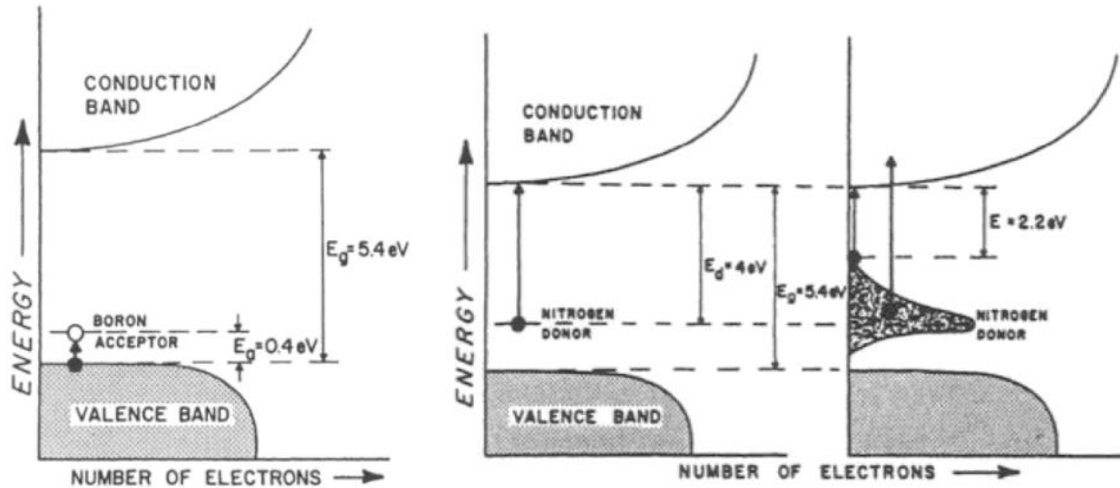


Figure 7: Band diagrams illustrating the boron acceptor energy level accepting electrons from the valence band maximum (left) and the nitrogen donor energy level donating electrons to the conduction band without the broadening shown (middle) and with broadening shown (right). Image taken from reference [52].

### 1.2.2.2 Surface Terminations

The diamond films formed by CVD are terminated with hydrogen. The typical CVD gas mixture primarily consists of hydrogen and consequently occupies a predominant number of the diamond surface sites. Therefore, in the CVD process the dangling carbon bonds are most likely to react with the atomic hydrogens at the surface sites, subsequently resulting in hydrogen-terminated diamond. The hydrogen termination preserves the  $sp^3$  diamond lattice and prevents graphitisation at the surface [38]. Alternatively, diamond films can be exposed to hydrogen plasma to produce a hydrogen-terminated surface. This hydrogen plasma treatment is also a commonly used method to clean diamond film surfaces and re-terminate the surface following oxidation. Hydrogen-terminated diamond has been demonstrated to have a negative electron affinity (NEA) (See Section 1.2.2.3).

Oxygen-terminated diamond is another common stable termination used in literature, which can be achieved by using an oxygen plasma or ozone exposure [53]. The different surface terminations on diamond can significantly affect the surface properties, changing the surface conductivity and the electron affinity vastly [54]. Oxygen-terminated diamond, in contrast to the hydrogen-terminated surface, exhibits a positive electron affinity.

### 1.2.2.3 Negative Electron Affinity

A material is defined to have a negative electron affinity (NEA) when the energy of the vacuum energy level is lower than the conduction band minimum, while the converse applies for a positive electron affinity (Figure 8) [55]. As the vacuum energy level is lower in energy than the conduction band, electrons donated into the conduction band can be emitted to the vacuum energy level without an energy barrier [56].

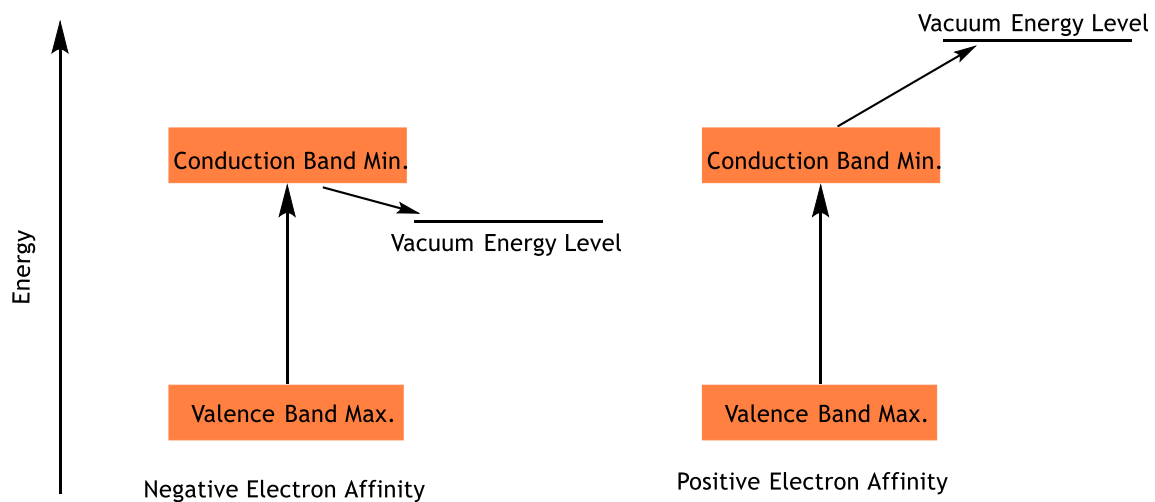


Figure 8: Simplified band diagrams for a material that exhibits a negative electron affinity (left) and a positive electron affinity (right).

The NEA in hydrogen-terminated diamond is induced by the surface dipole, resulting from hydrogen being less electronegative than the carbon in the diamond lattice [57]. The surface dipole subsequently causes the work function to decrease sufficiently, which produces the NEA property for the material. The electron affinity (EA) of a material can be determined from Equation 5 [58].

$$EA = \phi + (E_F - E_{VBM}) - E_{BG} \quad (5)$$

EA is the electron affinity,  $\phi$  is the work function of the material,  $E_F$  is the energy of the Fermi level,  $E_{VBM}$  is the energy of the valence band minimum, and  $E_{BG}$  is the energy of the band gap. Materials that can generate a stable negative electron affinity have the potential to be utilised in applications such as thermionic energy converters (See Section 1.3.1).

### 1.3 Underpotential Deposition Applied to Diamond

There have been few studies on the UPD of metals onto diamond. One study by Bouamrane *et al.* investigated Cu UPD onto diamond thin film electrodes [59]. Their research showed that an activation process was occasionally needed for the diamond electrode to exhibit UPD (Figure 9). The activation process involved polarising the electrode at -2.0 V for a few seconds and then cycling between 400 mV and 600 mV for a few minutes, measured with respect to a saturated calomel electrode (SCE) [59]. Prior to the activation step, no UPD was indicated for one electrode (Figure 9a). However, clear peaks in the UPD region of the cyclic voltammogram became visible after the electrochemical activation (Figure 9b), which signified the occurrence of UPD. For a different BDD electrode, which had the same pre-treatment, clear UPD peaks were present without the requirement of an activation step (Figure 9c).

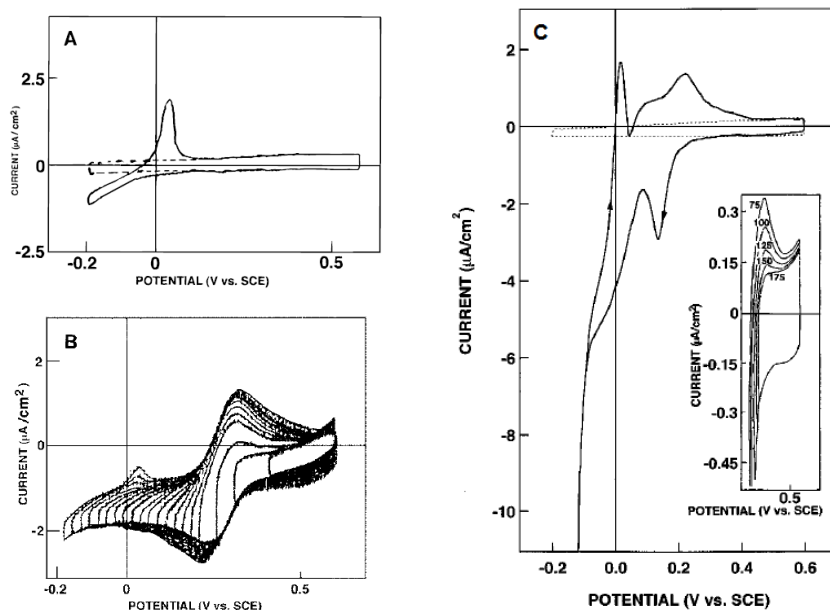


Figure 9: Cyclic current density-potential voltammograms for Cu UPD on BDD; (a) prior to activation in a 0.1 M H<sub>2</sub>SO<sub>4</sub> solution (dashed line) and a 0.1 M H<sub>2</sub>SO<sub>4</sub> + 1 mM CuSO<sub>4</sub> solution (solid line), (b) post electrochemical activation in a 0.1 M H<sub>2</sub>SO<sub>4</sub> + 1 mM CuSO<sub>4</sub> solution on the same BDD sample used in (a), and (c) without activation on a different BDD in a 0.1 M H<sub>2</sub>SO<sub>4</sub> solution (dashed line) and a 0.1 M H<sub>2</sub>SO<sub>4</sub> + 1 mM CuSO<sub>4</sub> solution (solid line). Image taken from reference [59].

Bouamrane *et al.* stated that the Cu monolayer formed at a low surface coverage of less than 2 % [59]. The interpretation given for the low monolayer coverage achieved was that the Cu UPD either only occurred on the graphitic carbon in the BDD electrode or alternatively at the polycrystalline grain boundaries [59].

Surface pre-treatment techniques are widely utilised to ‘activate’ the surface of electrodes. Various methods, including chemical, electrochemical and thermal pre-treatments, have been used to make electrodes electrochemically active [60]. The pre-treatments activate the electrode by exposing specific sites that allow electrons to be transferred at a faster rate. This occurs by removing surface contaminants, exposing a clean surface layer, or increasing the surface area through roughening [60]. Diamond electrode surfaces can be cleaned through plasma treatment processes. Alternatively, BDD

electrodes can be electrochemically activated. A hydrogen-terminated BDD electrode was demonstrated to exhibit enhanced electrochemical activity after a cathodic polarisation [61]. The cathodic polarisation activated the surface by replacing adsorbed oxygen with superficial hydrogens, increasing the number of active sites [60]. It was also reported that exposing a BDD electrode to alternating current pulses resulted in the electrochemical activation of the electrode [62].

The pH of a solution has been determined to significantly affect the surface charge of hydrogen- and oxygen-terminated diamonds. In neutral and basic solutions, hydrogen- and oxygen-terminated diamond were discovered to have a negative surface charge [63]. The negative surface charge on a diamond surface in a neutral solution would provide a more favourable Coulombic interaction between the diamond surface and metal ions. The more favourable Coulombic interactions in neutral solutions were hypothesised to encourage the formation of metal monolayers, aiding the occurrence of UPD. However, only a small number of studies have investigated UPD at a neutral pH. Recently, a study successfully demonstrated Cu UPD in a neutral solution of 2.5 mM CuSO<sub>4</sub> + 0.5 mM KCl on an Au(111) electrode [64]. Thus, it was hypothesised that a greater quantity of Cu would be underpotentially deposited onto a BDD film in a neutral solution of 2.5 mM CuSO<sub>4</sub> + 0.5 mM KCl compared to the more acidic solution used by Bouamrane *et al.* (0.1 M H<sub>2</sub>SO<sub>4</sub> + 1 mM CuSO<sub>4</sub>).

SLRR depositions expand the range of metal monolayers that can be deposited with high sensitivity. A successful SLRR deposition applied to a Cu UPD ad-layer on a BDD film would produce a more noble metal monolayer on the diamond surface. Therefore, various metal monolayers could be controllably deposited onto diamond surfaces if a SLRR deposition could be applied to a BDD. However, the coverage of a metal deposited in a SLRR process depends on the coverage of the 'sacrificial' UPD metal layer. This thesis investigated the Cu monolayer coverage that could be achieved by UPD on BDDs and subsequently the ability to use SLRR depositions to deposit more noble metal ad-layers. The ability to

deposit monolayer amounts of Cu and other metals onto diamond electrodes may facilitate advances in various applications, including thermionic energy converters (See Section 1.3.1) and electrocatalysis (See Section 1.3.2).

### **1.3.1 Thermionic emission**

Thermionic emission devices act as effective heat engines by converting external thermal energy applied at a hot cathode into electrical power (Figure 10) [65, 66]. Schlichter first conceived this as an alternative process to harvest renewable solar energy [65]. Thermal energy applied to the cathode increases the average kinetic energy of the electrons in the material sufficiently to overcome the material's work function. This results in electrons being emitted from the surface. The emitted electrons are collected at a cooler anode, which has a greater work function than the cathode, after travelling through a gas filled or vacuum interspatial region between the electrodes. The work function difference between the cathode and the anode instigates the electron transfer process, which subsequently generates a potential difference and induces the flow of electrons back towards the hot cathode to be reemitted. The resultant current is primarily driven by the thermal energy applied to the cathode and the work function difference between the two electrodes.

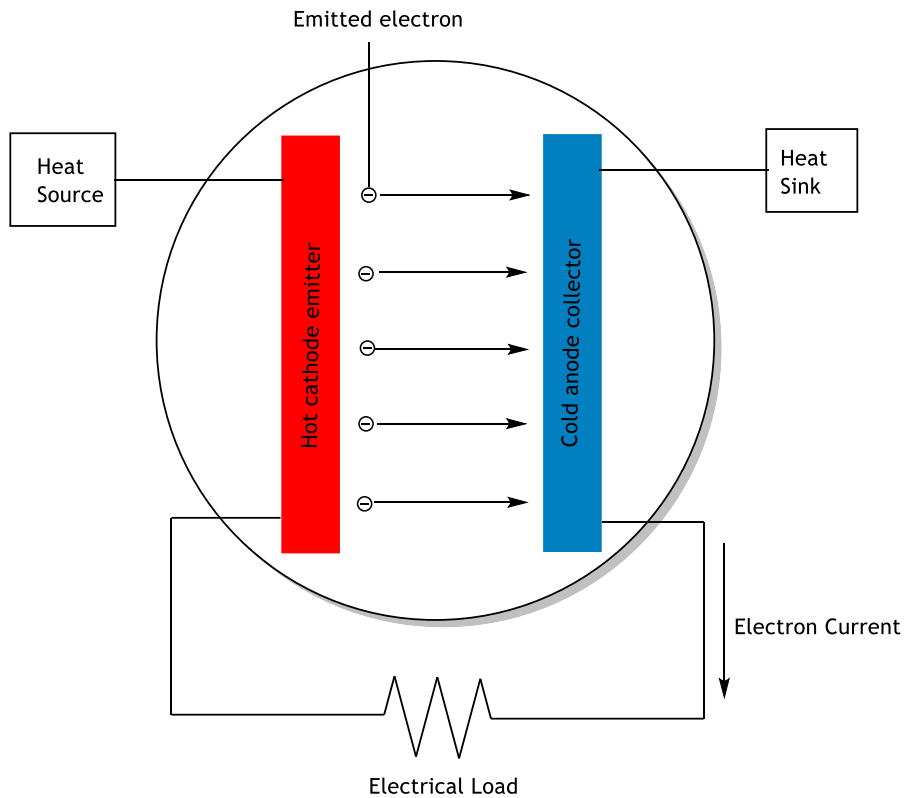


Figure 10: A representation of the process in a thermionic energy converter to generate electricity.

The use of thermionic energy converters has been restricted by the high operation temperatures required to produce appreciable currents and space charge developments between the electrodes in vacuum devices. Using a Cs-filled device provided many benefits, including mitigating the space charge effects [67, 68]. However, Cs is toxic and the cathode lifetime generally remains limited due to the cathode evaporating as a result of the extreme conditions [69]. These limitations have constrained the applicability of the thermionic energy converters to the space industry, which used thermionic energy converters to produce electrical energy for nuclear reactors on-board spacecrafts [70].

A successful thermionic energy converter would require the cathode emitter to have a small work function and a very high melting point. Thus, electronically conductive doped diamond became a particularly promising candidate as a low-temperature thermionic emitter as it can tolerate the extreme temperatures and exhibits a small effective work

function; as low as 0.9 eV for hydrogen-terminated *n*-type diamond due to its NEA [71]. The thermionic emission current of a doped diamond films is characterised by the Richardson equation (Equation 6) with increasing temperature until exceeding 750 °C, at which point emission current declines [72].

$$J = AT^2 e^{-\Phi/k_B T} \quad (6)$$

$J$  is the current density,  $A$  is the Richardson constant,  $\Phi$  is the work function of the diamond,  $k_B$  is the Boltzmann constant, and  $T$  is the temperature of the cathode.

The diminishing emission current coincides with hydrogen desorption from the diamond surface at temperatures over 500 °C [73]. The hydrogen desorption leads to a positive electron affinity and inhibits electron emission. Therefore, a hydrogen-terminated doped diamond is not a viable emitter for a thermionic energy converter as the hydrogen-terminated surface is not thermally stable at the ideal operating temperature.

Various studies have investigated alternative terminations and ad-layers that could also generate NEAs. These studies established that atomic layers of certain metals deposited on diamond have the potential to generate NEAs [74]. These developments led to research investigating metal-terminated BDD films that could facilitate a commercially viable thermionic energy converter.

Consequently, research has since determined a lithium-oxide-terminated doped diamond has great potential as a thermally stable thermionic emitter to function in solar thermionic energy conversion devices [71]. Theoretical studies into lithium-oxide-terminated diamonds have suggested that a NEA would be induced while exhibiting a high binding energy, up to 4.7 eV per Li atom [75]. This indicates that a LiO surface termination would have sufficient thermal stability required for a thermionic energy converter. Recently, a further theoretical study has also stated that C(001) diamond terminated by certain transition metal oxides (TMOs) in specific stoichiometries exhibit

large NEAs [73]. In addition, the thermal stability of the titanium-oxide-terminated diamond (Figure 11) was predicted to surpass that of H- and LiO-terminated diamond, requiring an estimated 7 eV to desorb  $\text{TiO}_2$  from the diamond surface or 7.60 eV to desorb Ti from the oxygen-terminated diamond [73]. Thus, a TiO-terminated diamond is an alternative candidate for a diamond emitter that could make thermionic energy converters achievable.

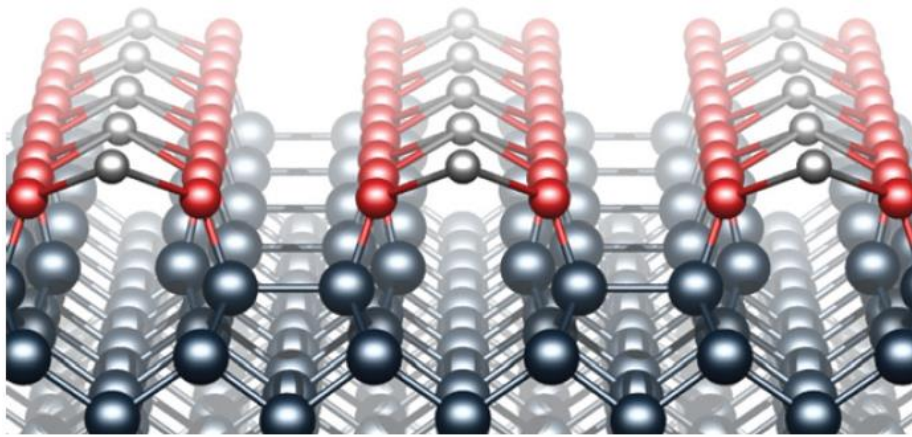


Figure 11: Representation of a diamond (001) surface with a chemisorbed layer of titanium oxide - black, red and grey spheres represent carbon, oxygen and titanium, respectively. Image taken from reference [73].

The current UHV deposition methods that are being explored have so far been unable to achieve the desired monolayer termination for a diamond emitter. These UHV techniques, including evaporation and subsequent deposition of metals, either deposit too much metal or deposit the metal in patches, which reduces the ability for the material to emit electrons. These shortfalls could be overcome if UPD was utilised, achieving a metal monolayer onto an oxygen-terminated diamond film. This method would be more sensitive to depositing the optimal monolayer termination than the UHV techniques. Thus, the feasibility of using UPD to attain the ideal monolayer termination on BDD films was investigated.

If the theoretical calculations can be reproduced practically, the initial aspiration for thermionic energy converters to provide a viable renewable energy source could be fulfilled. Despite the advances in forming diamond films with a thermally stable NEA, the ability to produce a feasible thermionic energy converter remains impeded by additional obstacles, including reducing the resistance within doped diamond films [71].

### 1.3.2 Electrocatalysis

In electrocatalysis it is imperative for electrodes to display high stability and exhibit minimal undesirable side reactions. Conventional metal electrodes and electrode supports are limited by undesired interfacial reactions and corrosion, unlike diamond because of the material's high chemical stability [76]. BDD electrodes have superior stability compared to conventional metal electrodes, resulting from the strong network of  $\sigma$ -bonds in diamond. Therefore, BDD electrodes have the potential to be significantly more versatile. Additionally, BDDs have properties of a low background current, weak adsorption of molecules, and a wide electrochemical window of polarizability in aqueous solutions [77, 78]. These features make BDDs a promising alternative material for use as a catalyst support.

The surface of BDD electrodes can be tuned for electrocatalytic applications by depositing metals onto the surface. Primarily the electrocatalysis studies of BDD electrodes have been focused on methanol oxidation for direct methanol fuel cells and water treatment applications [79, 80]. The diamond electrodes developed for methanol oxidation are modified at the surface to support a metal catalyst. Various techniques, from electrodeposition to microwave-assisted polyol synthesis, have been developed to load the metal and metal oxide catalysts, including Pt, Pt-based alloys, Pt/RuO<sub>2</sub> and Pt/TiO<sub>2</sub>, onto diamond [81, 82]. However, these techniques are unable to attain an epitaxial monolayer, which would ideally be achieved to optimise the catalyst for the electrocatalysis applications.

A monolayer termination of a catalytic metal on a BDD film would reduce the amount of catalytic metal used and could increase the catalyst durability. Thus, if UPD in conjunction with SLRR depositions can be used to accurately deposit a monolayer of catalytic metals onto BDD surfaces, it would optimise the catalyst coverage on the highly versatile BDD electrode. Moreover, this technique has the potential to pave the way for the development of further electrocatalysis applications involving BDD electrode supports as the loaded catalysts deposited via UPD could be formed in a variety of crystallographic structural arrangements. The various crystallographic structural arrangements potentially attainable could result in the altering of the catalytic behaviour, subsequently enabling wider electrocatalysis applications [83].

#### 1.4 Objectives

The objectives of this thesis were to determine whether UPD is a viable method to deposit a monolayer of metal onto doped diamond films and to indicate the potential applications in thermionic emission devices and electrocatalysis.

The objectives of this thesis were demonstrated by:

- Investigating Cu UPD on hydrogen-terminated hot filament chemical vapour deposition (HFCVD) and electrochemical grade BDD films in a 0.1 M H<sub>2</sub>SO<sub>4</sub> + 1.0 mM CuSO<sub>4</sub> solution.
- Investigating Cu UPD on an oxygen-terminated HFCVD BDD film in a 0.1 M H<sub>2</sub>SO<sub>4</sub> + 1.0 mM CuSO<sub>4</sub> solution.
- Investigating whether Cu UPD on hydrogen- and oxygen-terminated BDD films is more favourable at a more neutral pH.
- Investigating the application of SLRR based depositions of Pt using Cu UPD on a BDD film.

## Chapter 2: Experimental

### 2.1 Diamond

#### 2.1.1 Diamond Growth

Diamond films were grown in a HFCVD reactor on an *n*-type silicon wafer substrate (1 cm × 1 cm). The silicon substrate surface was abraded with 1-3 μm graded diamond powder (Diadust, Van Moppes) before being rinsed with methanol and subsequently dried with compressed air prior to the synthesis. The HFCVD reactor was run using tantalum wire filaments (0.25 mm diameter) 3 mm above the substrate surface. The process gases input into the reactor were diborane, methane and hydrogen at 0.071, 2, 200 sccm (standard cubic centimetre per minute), respectively. During the diamond growth the reactor was maintained at a constant temperature and pressure (~20 Torr) while a current of 25.0 A was sustained through the filament.

The diamond films were grown over two sets of 6 h. This produced two CVD-synthesised BDD film samples A and B, each with ~3 μm-thick BDD film on the silicon wafer. A two-point probe was used to determine that the samples had a similar resistivity between 0.25 - 1.05 kΩ (measured between opposite corners of the samples).

The diamond films were submerged in hot nitric acid (60 °C) for 10 mins to ensure the absence of impurities and rinsed with ultrapure Milli-Q water before being dried with Ar gas.

Raman spectroscopy and scanning electron microscopy (SEM) were used to characterise the BDD films.

#### 2.1.2 Electrochemical Grade Diamonds

Electrochemical grade BDD diamond film, with a high boron concentration in the range of 2 to 6 × 10<sup>20</sup> atoms cm<sup>-3</sup>, was purchased from Element Six [84]. The film was refluxed in a 100 ml solution containing KNO<sub>3</sub> (6.5 g) and 95 % H<sub>2</sub>SO<sub>4</sub> (both purchased from Sigma

Aldrich) to remove any contaminants and were then dried with Ar gas. The electrochemical grade diamond film was then characterised using SEM and hydrogen-terminated in a hydrogen plasma reactor (See Section 2.2.1).

A two-point probe was used to determine that the sample had a resistivity of 18.9  $\Omega$  (measured between two opposite corners of the sample).

## **2.2 Termination Techniques**

### **2.2.1 Hydrogen plasma termination**

The BDD films were hydrogen-terminated in a microwave plasma CVD reactor. The hydrogen was flowed into the reactor at 300 sccm. The samples were held initially at a pressure of 80 Torr while 1200 W were applied for 2 mins - equating to a substrate temperature  $\sim 900$  °C. Subsequently, the pressure and electrical power were reduced to 40 Torr and 750 W for 2 mins, leading to a substrate temperature  $\sim 550$  °C. The samples were allowed to cool at 40 Torr, while hydrogen flow was maintained, for a further 2 mins.

All the diamond samples were hydrogen-terminated in a microwave plasma reactor after being submerged in hot acid or acid refluxed to ensure the surface was clean and hydrogen-terminated. Sample A was then used for the electrochemical deposition investigations onto a hydrogen-terminated BDD film surface, while sample B was also hydrogen-terminated to clean the surface of contaminants prior to an oxygen termination procedure (See Section 2.2.2 and 2.2.3). Subsequently, sample B was used for electrochemical deposition investigations onto an oxygen-terminated BDD film surface.

### **2.2.2 Oxygen plasma termination**

The oxygen termination in the oxygen plasma reactor was achieved after exposure to an oxygen plasma for 10 s. The reactor was operated at a pressure and voltage of 0.7 Torr and  $\sim 1.35$  kV, respectively, while the oxygen was flowed into the reactor at 10 sccm.

Sample B was oxygen-terminated using the oxygen plasma reactor for the first electrochemical experiment. However, due to that unavailability of the reactor, a different oxygen termination procedure using ozone exposure in UV was required for the next oxygen termination (See Section 2.2.3).

### **2.2.3 Ozone exposure in UV**

A UVO cleaner was used to expose the diamond surface of sample B to ozone in UV, which generated atomic oxygen to terminate the surface. This surface termination was run for 30 mins to ensure full oxygen surface coverage.

Sample B was oxygen-terminated with this method following on from the first electrochemical deposition experiment.

## **2.3 Electrochemical Experiments**

### **2.3.1 Copper Underpotential deposition**

Cyclic voltammetry Cu UPD experiments were conducted under nitrogen deaeration in a three-electrode cell using either hydrogen- or oxygen-terminated BDD films as the working electrodes, Pt wire as a counter electrode and Cu wire ( $\text{Cu}/\text{Cu}^{2+}$ ) as the reference electrode.

Cu UPD was investigated in a 0.1 M  $\text{H}_2\text{SO}_4$  + 1.0 mM  $\text{CuSO}_4$  solution for samples A, B and the hydrogen-terminated electrochemical grade diamond.

Prior to further electrochemical depositions in more neutral solutions, samples A and B were both re-terminated with hydrogen and oxygen, via ozone exposure, respectively (See Section 2.2). Electrochemical deposition experiments were then investigated in a 2.5 mM  $\text{CuSO}_4$  solution, pH 5, followed by a 2.5 mM  $\text{CuSO}_4$  + 0.5 mM KCl solution, pH 6.

Before all electrochemical experiments, the diamonds were submerged in 95 % H<sub>2</sub>SO<sub>4</sub> for 10 mins to remove surface contaminants, and thoroughly rinsed with ultrapure Milli-Q water. The Cu and Pt electrodes were cleaned in 70 % HNO<sub>3</sub> for 10 s, thoroughly rinsed with ultrapure Milli-Q water and dried with N<sub>2</sub> before each experiment. Additionally, the Pt electrode was flash flame annealed just before inserting into the cell.

Cu was underpotentially deposited on sample A, at 0.080 V vs. Cu/Cu<sup>2+</sup> for 5 mins, in a 2.5 mM CuSO<sub>4</sub> solution. The Cu covered BDD film was rinsed with ultrapure Milli-Q water and then dried with N<sub>2</sub> before characterisation using X-ray photoelectron spectroscopy (XPS).

### **2.3.2 Surface-limited redox replacement (SLRR) deposition of Pt**

Cu was underpotentially deposited onto sample A (which had been re-terminated prior to the experiment) in 2.5 mM CuSO<sub>4</sub> at 0.080 V vs. Cu/Cu<sup>2+</sup> for 5 mins. The Cu UPD ad-layer was replaced with Pt in a SLRR deposition in a solution of 0.5 mM K<sub>2</sub>PtCl<sub>4</sub> + 0.1 M HClO<sub>4</sub>, while maintaining the N<sub>2</sub> environment. The BDD was in the Pt solution until the open-circuit potential stabilised, for ~45 mins. After the SLRR deposition was completed, a CV was run in a 2.5 mM CuSO<sub>4</sub> solution on the Pt covered sample.

Cu of an equivalent charge to a monolayer was deposited onto the hydrogen-terminated electrochemical grade BDD film at a low overpotential, -0.120 V vs. Cu/Cu<sup>2+</sup> for 17 s, in 2.5 mM CuSO<sub>4</sub>. The electrochemical grade BDD film was re-terminated prior to the experiment. The Cu deposit was replaced with Pt in a SLRR deposition, performed identical to that described above. Afterwards, a CV was also run in a 2.5 mM CuSO<sub>4</sub> solution.

The Pt deposit on sample A was characterised using XPS after being rinsed with ultrapure Milli-Q water and then dried with N<sub>2</sub>. While the Pt deposit on the hydrogen-terminated electrochemical grade BDD film was characterised using SEM and XPS after also being rinsed with ultrapure Milli-Q water and then dried with N<sub>2</sub>.

## Chapter 3: Results and Discussion

### 3.1 Characterisation of Diamond Films

#### 3.1.1 HFCVD Diamond Films

SEM and Raman spectroscopy were used to prove that the HFCVD diamond growth was successful and to determine the quality of films. The SEM images illustrated that polycrystalline diamond (crystal size  $\sim 0.7 - 3.6 \mu\text{m}$ ) was visible on the silicon wafer substrates, as shown in Figure 12 and 28. Raman spectroscopy, using a green 514 nm laser, evidently showed a sharp peak at  $1329 \text{ cm}^{-1}$  that is characteristic of the first-order band corresponding to  $sp^3$  hybridised carbon (Figures 13 and 29) [85]. A bulge in the intensity with a peak at  $1554 \text{ cm}^{-1}$  was also apparent in Figures 13 and 29. The bulge correlated to  $sp^2$  hybridised carbon, referred to as the G peak [86]. This indicated that a small quantity of graphite was included in the diamond films, although at a low concentration. The distinctive diamond peak was observed to be asymmetric. The asymmetry of the peak occurs due to the Fano effect resulting from the inclusion of boron in the diamond lattice [86].

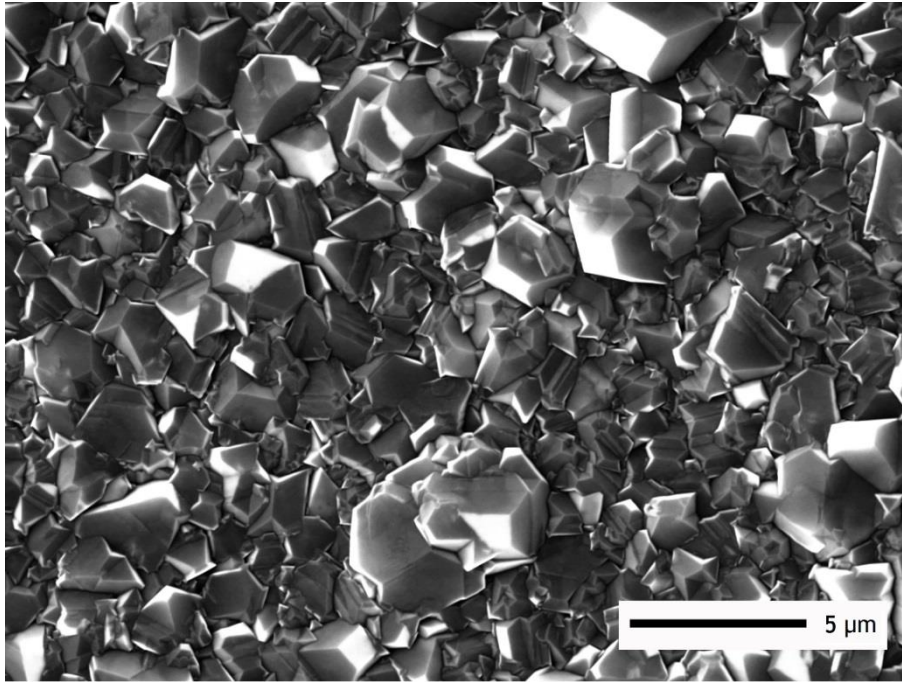


Figure 12: SEM image of a boron-doped diamond film, denoted sample A, synthesised in a hot filament CVD reactor.

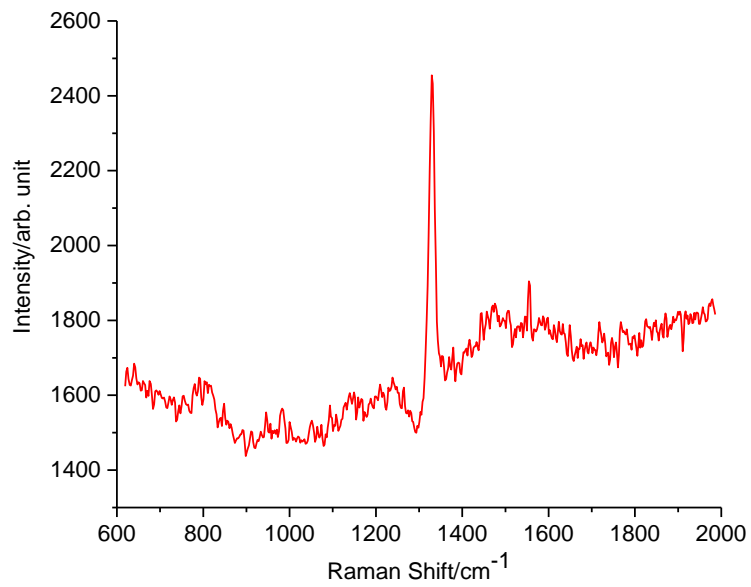


Figure 13: Raman spectrum using a green 514 nm laser of a boron-doped diamond film, denoted sample A, synthesised in a hot filament CVD reactor.

The SEM images and Raman spectra conclusively demonstrated that the HFCVD diamond films were successfully synthesised and of a quality that is typically reported in literature [87]. The grain boundaries in polycrystalline diamond films provide sites in which less diamond-like material is located between the crystals [88]. Consequently, the graphitic carbon was most likely located at the polycrystalline grain boundaries.

### **3.1.2 Electrochemical Grade Diamond Films**

The electrochemical grade BDD film surface was also characterised by SEM. These diamond films possessed a roughened side and a smooth polished surface on the opposite side, which were identified in SEM Figures 14 and 30, respectively. The roughened side of the electrochemical grade BDD faced the counter and reference electrodes for the electrochemical experiments because the surface was more comparable to the HFCVD synthesised polycrystalline BDD films, as opposed to the smooth polished side. However, the crystal faces exposed on the electrochemical grade diamond's roughened side were larger than that of the HFCVD synthesised diamond films (Figure 12).

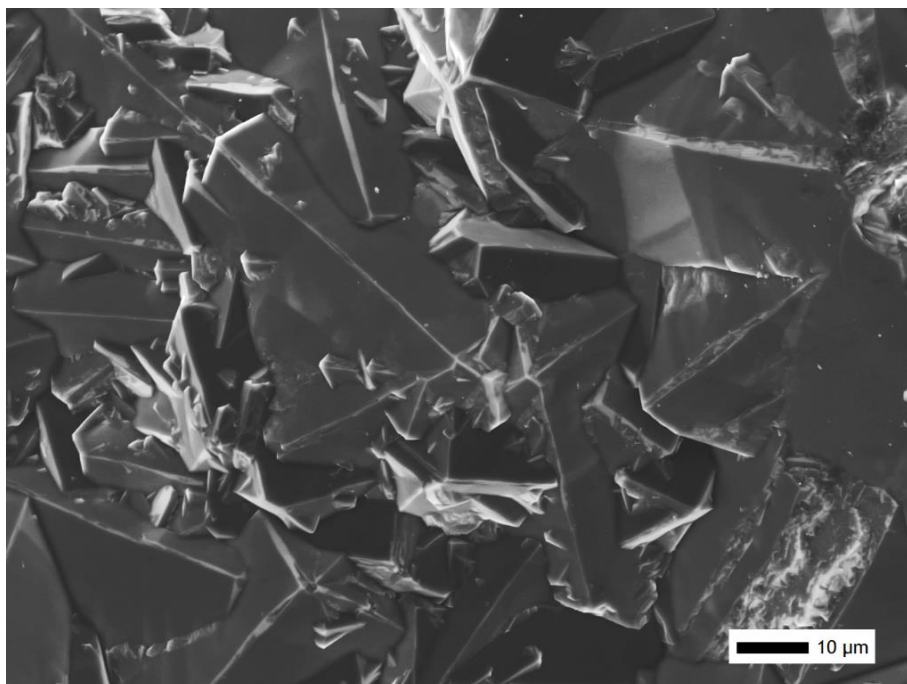


Figure 14: SEM image of the roughened side of the electrochemical grade boron-doped diamond film.

The electrochemical grade BDDs had a significantly higher boron concentration compared to the HFCVD synthesised BDDs. The high boron concentration in the electrochemical grade diamond (in the range of  $2$  to  $6 \times 10^{20}$  atoms  $\text{cm}^{-3}$ ) was used to investigate whether the Cu UPD was influenced by the conductivity of the BDD electrode.

## 3.2 Cu Underpotential Deposition

### 3.2.1 Hydrogen-terminated Diamond Films

#### 3.2.1.1 Solution: $0.1 \text{ M H}_2\text{SO}_4 + 1 \text{ mM CuSO}_4$

Cu UPD on sample A was undertaken in a  $0.1 \text{ M H}_2\text{SO}_4 + 1 \text{ mM CuSO}_4$  solution in order to replicate Bouamrane *et al.*'s work (Figure 15) [59]. However, this research used a Cu wire ( $\text{Cu}/\text{Cu}^{2+}$ ) (0.34 vs. standard hydrogen electrode) as the reference electrode rather than a SCE (0.24 vs. standard hydrogen electrode) [100]. There was no indication of a peak in the

UPD region without an activation process, only a bulk stripping peak at 0.03 V. Following the same activation process that was used by Bouamrane *et al.* involving a cathodic polarisation, a peak in the UPD region during the stripping of the CV was identified at 0.16 V, as shown in Figure 15. The small UPD peak indicated that a small charge transfer occurred, and thus a low quantity of Cu was underpotentially deposited. No corresponding UPD peak for the deposition of the Cu onto the BDD film was apparent.

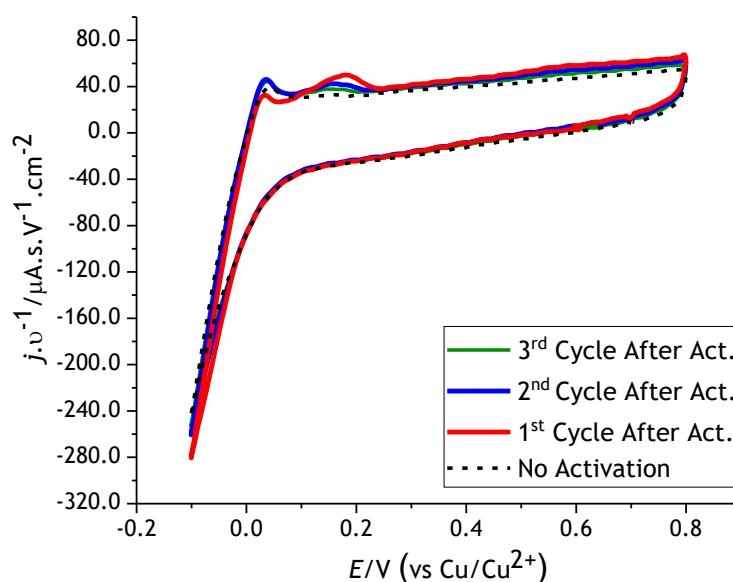


Figure 15: Cyclic voltammograms with sample A as the working electrode in a 0.1 M H<sub>2</sub>SO<sub>4</sub> + 1 mM CuSO<sub>4</sub> solution - scan rate 50 mV s<sup>-1</sup>. The activation process involved a cathodic polarisation at -2.10 V for 3 s and a subsequent cycling between 0.40 V and 0.60 V for 2 mins.

The low quantity of Cu UPD showed that the interactions between the Cu ad-layer and the BDD surface were not particularly favourable in the conditions used. Thus, the electron transfer across the interface was only favourable for the Cu deposition at the most energetically favourable sites. Consequently, the low quantity of Cu deposition most likely

corresponded to random deposition into the crystal defects and polycrystalline grain boundaries, which are the most energetically favourable surface sites.

The Cu UPD deposition peak was not visible. The absence of the peak was attributed to the slow deposition of Cu over a broad potential range, suggesting that the process was potentially kinetically controlled. Accordingly, as a low quantity of charge was transferred over a broad potential range, an obviously identifiable peak in the current density was not displayed. In contrast, the stripping peak was apparent because the Cu UPD ad-layer was completely stripped from the BDD surface over a small potential range at 0.16 V.

The Cu UPD stripping peak has been shown to initially decrease after the first cycle, while the bulk peak at 0.03 V increases. The observed changes can be correlated with the initial structural changes that occur in the deposition of the Cu ad-layer and potential inhibition of the activated available sites over time.

The appearance of the UPD peak is dependent on the cathodic polarisation at  $-2.10$  V and subsequent cycling between  $0.40$  V and  $0.60$  V (vs.  $\text{Cu}/\text{Cu}^{2+}$ ). Previous studies have suggested that the cathodic polarisation favourably alters the BDD surface. The favourable alteration of the BDD surface has been ascribed to the conversion of some C-O functionalities into C-H functionalities [60]. This surface modification was supported by the experimental observation that bubbles, presumably of hydrogen, formed on the surface of the film during the cathodic polarisation. The purpose of cycling between  $0.40$  V and  $0.60$  V (vs.  $\text{Cu}/\text{Cu}^{2+}$ ) was to remove Cu that was bulk deposited during the cathodic polarisation. The emergence of the UPD peak after the polarisation and the experimental observation supported the occurrence of the surface modification. This modification was suggested to lead to an increase in the number of active sites available for Cu to deposit as a greater surface area of the BDD film was hydrogen-terminated. However, confirmation and quantification of the surface change was unable to be achieved.

Even though the procedure described in Bouamrane *et al.*'s paper was followed, the results obtained did not replicate their published results (Figure 9) [59]. In comparison with their results, a smaller UPD stripping peak at a less positive potential was observed and no comparable UPD deposition peak was identifiable. This signified that a lower quantity of Cu UPD occurred than expected because a lower quantity of charge was transferred. Also, the shift in the potential of the UPD stripping peak suggested that there was a higher energetic barrier for the electron transfer to overcome than in the system shown in Figure 9.

The lower quantity of Cu UPD and greater energetic barrier relative to the system in Figure 9 could be ascribed to a change in the surface quality of the BDD electrode. A change in the surface quality could have led to less energetically available active sites for the Cu to underpotentially deposit. The surface quality of an electrode is affected by adsorbed contaminants on the surface as well as oxidation of the hydrogen-terminated surface. The number of contaminants on the surface of the BDD electrode used was assumed to be similar to the electrodes used by Bouamrane *et al.* as the same cleaning procedure was followed. Therefore, oxidation of the hydrogen-terminated electrode surface was expected to have altered the surface quality to a greater extent than the presence of surface contaminants. The grain boundaries in polycrystalline diamond are established to be occupied by less diamond-like material and consequently are more susceptible to oxidation; up to 100× faster than diamond single-crystal (100) faces [88]. Thus, the 19 days between the hydrogen plasma termination of the BDD electrode and its use in the electrochemical experiment may have enabled the oxidation of the polycrystalline grain boundaries. Provided the oxidised surface hindered Cu UPD, the increased oxidation of the BDD film would account for the decrease in the Cu UPD observed and the potential shift relative to the expected results.

Cu UPD onto a hydrogen-terminated electrochemical grade BDD film in a 0.1 M H<sub>2</sub>SO<sub>4</sub> + 1 mM CuSO<sub>4</sub> solution was analysed. After the cathodic activation at -2.10 V (vs. Cu/Cu<sup>2+</sup>)

and subsequent cycling to remove the bulk deposited Cu, similar graphical features to the Cu UPD on sample A were observed; a Cu UPD stripping peak at 0.21 V and no definitive UPD deposition peak (Figure 16). However, the CV of the Cu UPD region showed a larger background current with the electrochemical grade diamond film as the working electrode compared to the CV that used a HFCVD synthesised BDD film (Figure 15).

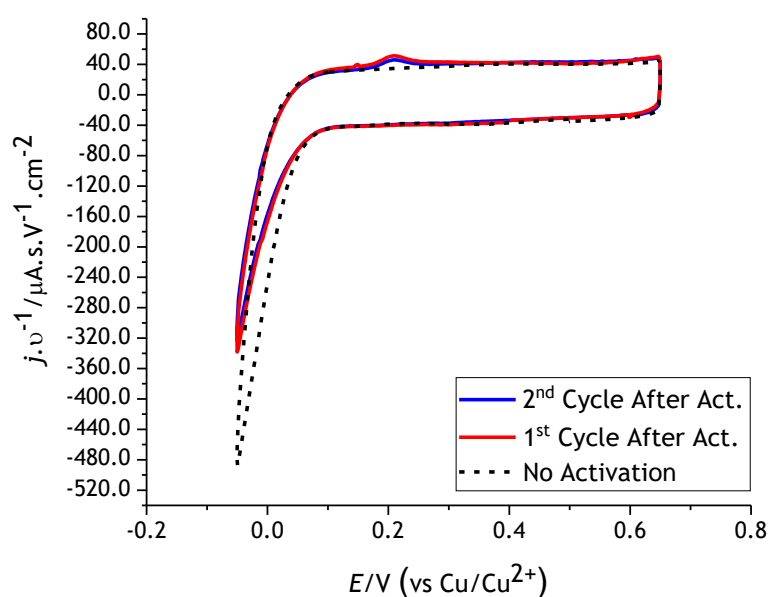


Figure 16: Cyclic voltammograms with a hydrogen-terminated electrochemical grade BDD film as the working electrode in a 0.1 M  $\text{H}_2\text{SO}_4$  + 1 mM  $\text{CuSO}_4$  solution - scan rate  $50 \text{ mV s}^{-1}$ . The activation process involved a cathodic polarisation at  $-2.10 \text{ V}$  for 3 s and a subsequent cycling between 0.40 V and 0.60 V for 2 mins.

The greater background current is correlated to the increased capacitance of the electrode. The greater capacitance current exhibited by the electrochemical grade BDD film was attributed to the increased boron concentration relative to the HFCVD synthesised film, as well as an increase in the surface area of BDD film exposed to the solution [89]. A greater surface area of the electrochemical grade BDD film was exposed to the solution because it possessed a rougher surface than the HFCVD synthesised BDD film. Apart from the increased background current, the increased doping of the electrochemical

grade BDD film was shown not to have a significant influence on Cu UPD onto a BDD surface.

#### **3.2.1.2 Solution: 2.5 mM CuSO<sub>4</sub>**

In the 2.5 mM CuSO<sub>4</sub> solution, Cu UPD peaks were exhibited at 0.12 V and 0.26 V (Figure 17). The peak at 0.07 V corresponded to the stripping of the bulk deposited Cu from the electrode. The UPD phenomenon did not require an activation process to exhibit the UPD peaks. However, the UPD peaks exhibited a small current, which suggested a small amount of charge was transferred, albeit more than in the 0.1 M H<sub>2</sub>SO<sub>4</sub> + 1 mM CuSO<sub>4</sub> solution. Subsequently, only a small quantity of Cu was underpotentially deposited onto the BDD film. This was at a quantity significantly less than a monolayer, which ideally would have been achieved. The UPD stripping peak was present at a more positive potential than in the 0.1 M H<sub>2</sub>SO<sub>4</sub> + 1 mM CuSO<sub>4</sub> solution. The positive potential shift of the stripping peak indicated that the UPD ad-layer was more stabilised in the 2.5 mM CuSO<sub>4</sub> solution. The increased Cu UPD in the more neutral solution coincided with the more favourable Coulombic interactions, which were hypothesised to encourage UPD.

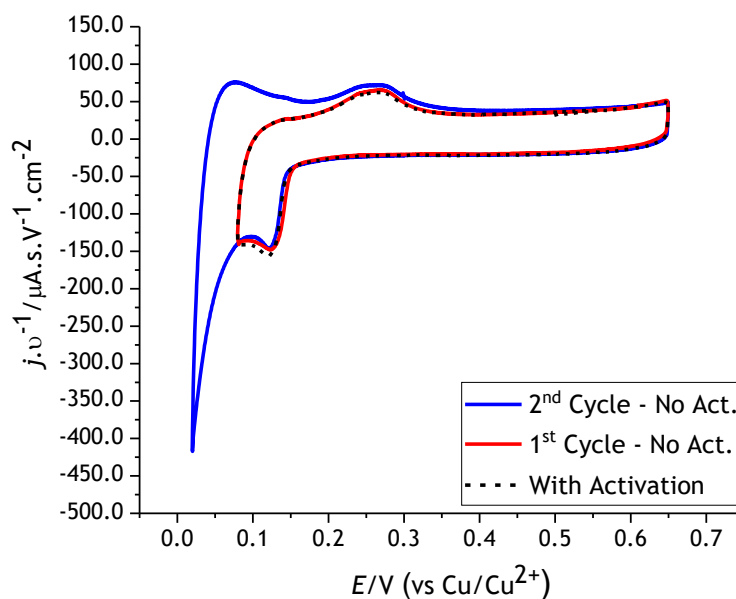


Figure 17: Cyclic voltammograms with sample A as the working electrode in a 2.5 mM  $\text{CuSO}_4$  solution - scan rate  $20 \text{ mV s}^{-1}$ . The activation process involved a cathodic polarisation at  $-2.10 \text{ V}$  for 3 s and a subsequent cycling between  $0.40 \text{ V}$  and  $0.60 \text{ V}$  for 2 mins.

The peaks in the UPD region were definitively associated with the UPD phenomenon rather than bulk deposition. This determination was achieved by cycling to a lower potential, which did not result in an enlargement of the peaks relating to Cu UPD (Figure 17). This is a diagnostic feature of UPD peaks as UPD is a surface adsorption-like process, which can deposit only until all energetically available surface sites are occupied. This differs from bulk deposition as a bulk associated peak increases upon cycling to lower potentials.

The Cu UPD stripping peak in the 2.5 mM  $\text{CuSO}_4$  solution are shifted to a more positive value compared with the Cu UPD stripping peak experimentally recorded in  $0.1 \text{ M H}_2\text{SO}_4 + 1 \text{ mM CuSO}_4$ , Figure 15. The shift of the peak to a more positive potential indicated that the Cu ad-layer was more stabilised in the 2.5 mM  $\text{CuSO}_4$  solution, assuming the same UPD process occurred and that the surface quality of the electrode was the same [90]. Thus, considering the experimentally obtained results, a greater quantity of Cu UPD was

demonstrated in the 2.5 mM CuSO<sub>4</sub> solution, which supported the hypothesis that the more favourable Coulombic interactions in more neutral solutions encourage UPD.

The Cu UPD deposition and stripping peaks in Figure 17 are clearly identifiable and comparable to the results obtained by Bouamrane *et al.* in Figure 9b and c. The peaks in Figure 17 are shifted to slightly less positive values relative to those shown in Figure 9b and c. The shift of the peaks can be accounted for as a result of using a Cu wire reference electrode rather than a SCE. Additionally, the greater concentration of Cu<sup>2+</sup> ions in the 2.5 mM CuSO<sub>4</sub> solution is another contributing factor that would have influenced the peak position [91]. The UPD peaks published by Bouamrane *et al.* were shifted to different potentials for each different electrode (Figure 9) [59]. Thus, the peak shifts can also be related to the unusual nature of the polycrystalline diamond electrodes, as well as the quality of the hydrogen-terminated surface.

A cathodic polarisation was not required to observe UPD in the 2.5 mM CuSO<sub>4</sub> solution. The lack of a prerequisite treatment process illustrated that the specific surface sites where Cu UPD occurred were already activated, or alternatively less inhibited. Thus, the activation process had a redundant effect on Cu UPD in the 2.5 mM CuSO<sub>4</sub> solution (Figure 17). This was in significant contrast to the Cu UPD in the 0.1 M H<sub>2</sub>SO<sub>4</sub> + 1 mM CuSO<sub>4</sub> solution, in Figure 15, which required an activation process to exhibit UPD. As UPD is particularly sensitive to the electrode surface, any contamination or variation in the surface quality could account for the dependence of UPD in the 0.1 M H<sub>2</sub>SO<sub>4</sub> + 1 mM CuSO<sub>4</sub> solution on the activation process.

The electrochemical experiment in the 2.5 mM CuSO<sub>4</sub> solution was undertaken 24 h after the surface of sample A was hydrogen-terminated. This time delay was minimal compared to the 19 days between the hydrogen termination of sample A and its use in the electrochemical experiment in the 0.1 M H<sub>2</sub>SO<sub>4</sub> + 1 mM CuSO<sub>4</sub> solution. The extended time delay in the electrochemical deposition investigation in the 0.1 M H<sub>2</sub>SO<sub>4</sub> + 1 mM CuSO<sub>4</sub>

solution would have enabled greater oxidation of the hydrogen-terminated BDD film surface to occur. As stated previously, the oxidation of the diamond film takes place most readily at the polycrystalline grain boundaries, which are the most favourable deposition sites for the Cu to deposit. Therefore, the increase in Cu UPD observed and the peak shift in the 2.5 mM CuSO<sub>4</sub> solution, relative to 0.1 M H<sub>2</sub>SO<sub>4</sub> + 1 mM CuSO<sub>4</sub> solution, was correlated to the more favourable Coulombic interaction between the BDD film and the Cu<sup>2+</sup> ions, as well as the better surface quality of the electrode. However, it was undetermined which factor had greater influence in increasing the Cu UPD.

### **3.2.1.3 Solution: 2.5 mM CuSO<sub>4</sub> + 0.5 mM KCl**

The CV of the Cu UPD region in the solution of 2.5 mM CuSO<sub>4</sub> + 0.5 mM KCl (Figure 18) did not produce the similarly stable UPD peaks recorded in the 2.5 mM CuSO<sub>4</sub> solution. Instead, only a UPD stripping peak was displayed at 0.20 V after the activation process, which involved a cathodic polarisation at -2.10 V (vs. Cu/Cu<sup>2+</sup>). Thus, this replicated the results obtained in the 0.1 M H<sub>2</sub>SO<sub>4</sub> + 1 mM CuSO<sub>4</sub> solution (Figure 15).

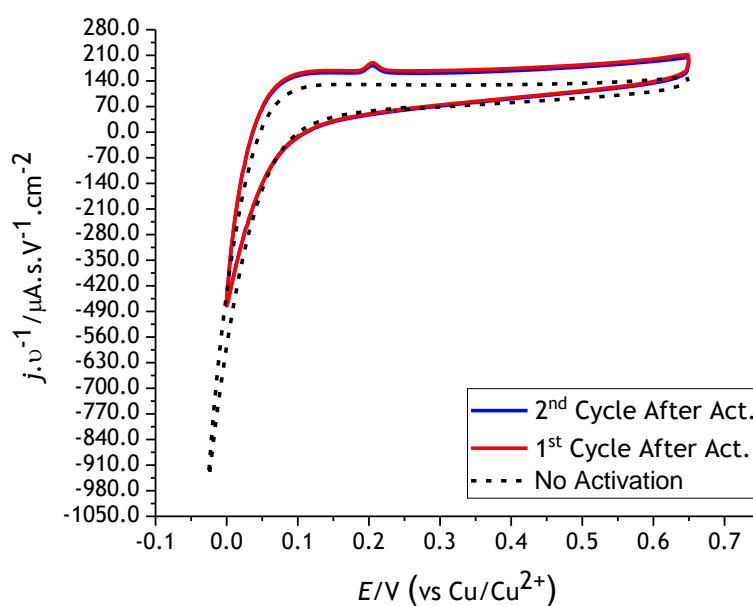


Figure 18: Cyclic voltammogram with sample A as the working electrode in a 2.5 mM  $\text{CuSO}_4$  + 0.5 mM KCl solution - scan rate  $20 \text{ mV s}^{-1}$ . The activation process involved a cathodic polarisation at  $-2.10 \text{ V}$  for 3 s and a subsequent cycling between  $0.40 \text{ V}$  and  $0.60 \text{ V}$  for 2 mins.

The Cu UPD peak in the 2.5 mM  $\text{CuSO}_4$  + 0.5 mM KCl solution was distinctively similar to the results obtained in the 0.1 M  $\text{H}_2\text{SO}_4$  + 1 mM  $\text{CuSO}_4$  solution rather than the 2.5 mM  $\text{CuSO}_4$  solution. Therefore, it was rationalised that the change in the CV, compared to the result obtained in the 2.5 mM  $\text{CuSO}_4$  solution, was attributed to either the addition of KCl in the electrolyte or a variation in the electrode surface quality.

Diamond electrodes have been shown to display unusual electrochemical behaviour in KCl electrolytes. Nevertheless, this has not been conclusively explained [93]. However, additional interaction between the  $\text{Cl}^-$  ions and the BDD film as well as  $\text{Cl}^-$  ions complexing with the  $\text{Cu}^{2+}$  ions could have decreased the favourability of forming a Cu ad-layer [92]. Despite the more favourable Coulombic interaction hypothesised in the more neutral solution, these additional interactions in the KCl electrolyte solution could potential account for the reduction in Cu UPD observed.

Alternatively, the reduction in the Cu UPD observed could be associated with the oxidation of the BDD film prior to use in the electrochemical investigation. The oxidation of the BDD film would maintain the hypothesised favourable Coulombic interaction but decrease the favourability of the electron transfer to the  $\text{Cu}^{2+}$  ions [94]. Therefore, the partial oxidation of the surface sites would result in a decrease in the energetically available sites for Cu UPD to occur. The time between the surface termination and the electrochemical investigation was 15 days. This time delay between the termination of the surface and use in electrochemical deposition experiment may have been sufficient for partial oxidation in the polycrystalline grain boundaries. Hence, oxidation of the surface would have contributed to the reduction in UPD observed as long as the oxidation of the surface inhibited Cu UPD.

The addition of KCl and the decreased quality of the electrode would have both contributed to the decrease in the Cu UPD observed in comparison with the UPD achieved in the 2.5 mM  $\text{CuSO}_4$  solution. However, the oxidation of the surface was determined to have a more profound effect in decreasing Cu UPD than the addition of KCl. This is because the UPD achieved was similar to that in the 0.1 M  $\text{H}_2\text{SO}_4$  + 1 mM  $\text{CuSO}_4$  solution after the cathodic polarisation, which presumably replaced C-O functionalities on the surface into C-H functionalities. Subsequently, the dependence of UPD on the activation process indicated that C-O functionalities on the surface were the most significant factor inhibiting the Cu UPD.

Comparing the UPD achieved in the three solutions, the quantity of Cu UPD decreased as the time between the hydrogen termination of sample A and its use in the electrochemical investigations increased. This correlation illustrated that the surface quality of the electrode decreased with time, as the electrode surface oxidised. Therefore, ensuring the electrode surface has not been oxidised is a pivotal factor in obtaining Cu UPD on a hydrogen-terminated BDD film. Additionally, the increased favourable Coulombic interactions between the BDD surface and the metal ions appeared to aid the occurrence

of UPD. However, further investigations would be required to fully establish the influence that the more favourable Coulombic interactions have on encouraging UPD on BDD films.

#### 3.2.1.4 X-ray Photoelectron Spectroscopy (XPS)

Cu UPD, deposited in 2.5 mM CuSO<sub>4</sub>, on sample A was analysed using XPS. The sample was not heated prior to the XPS to ensure the Cu ad-layer did not evaporate from the surface. The XPS analysis clearly identified C 1s, O 1s and two Cu peaks at 284, 533, 952 and 933 eV in the survey scan, respectively (Figure 19) [95]. The Cu peaks corresponded to the Cu 2p (1/2) and 2p (3/2) (Figure 20) [95]. Trace impurities of Si were also detected. This impurity may have originated from the Si substrate.

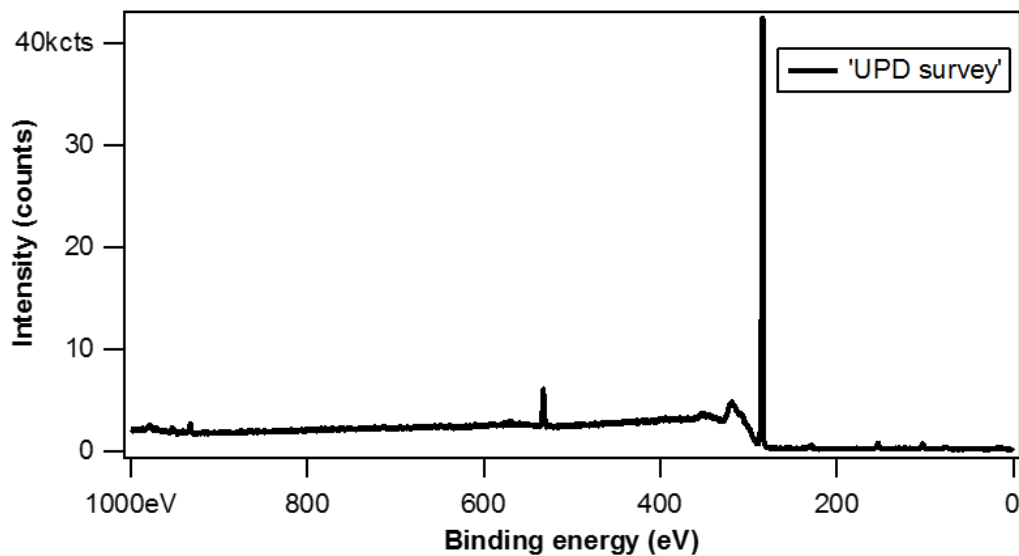


Figure 19: XPS survey scan of the Cu UPD ad-layer on sample A from 0 to 1000 eV.

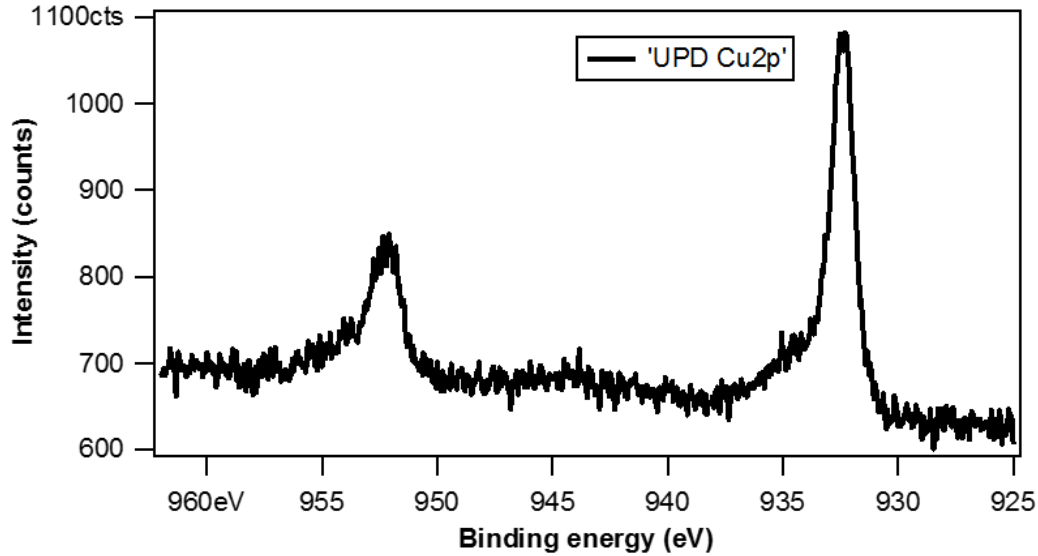


Figure 20: XPS spectrum of the Cu 2p peaks of the Cu UPD ad-layer on sample A.

The presence of the Cu peaks proved that Cu was underpotentially deposited onto the BDD surface. The Cu ad-layer remained relatively air stable as it was not completely etched from the surface between deposition and analysis. The Cu peak intensities were determined to represent a ~2 % monolayer coverage on the BDD film surface. This evaluation agreed with the amount of Cu UPD estimated by Bouamrane *et al.* [59]. The low quantity of Cu UPD correlated to the small Cu UPD peaks observed in the 2.5 mM CuSO<sub>4</sub> solution, and thus the small quantity of charge transferred (Figure 17). The 2 % monolayer coverage corresponded to the coverage expected had the Cu only been deposited at the polycrystalline grain boundaries of the BDD film.

The Raman spectra (Figures 13 and 29) identified graphitic carbon present in the BDD films polycrystalline grain boundaries. Thus, the Cu deposited could correspond to the Cu deposition onto graphitic carbon rather than diamond *sp*<sup>3</sup> carbon [59]. However, it was not established whether the Cu was deposited onto the graphite or diamond, although the Cu was assumed to deposit on the diamond *sp*<sup>3</sup> carbon.

The oxygen peak present was attributed to the oxidation of the Cu deposit and the diamond film surface. The identification of the O peak supports the inference that oxidation of the film had occurred and altered the quality of the electrode surface over time. This further supported the conclusion that the time between the hydrogen termination procedure and an electrode's use in the electrochemical experiments is an important factor to maintain a high-quality hydrogen-terminated surface.

Despite minimal time between the termination and deposition in the 2.5 mM CuSO<sub>4</sub> solution, Cu UPD was only indicated to be achievable at a low monolayer coverage. The low UPD metal monolayer coverage currently shown to be attainable onto a BDD film makes it an unfeasible method to deposit an electrocatalyst on a BDD or to synthesise a thermionic emitter. However, this conclusion is not definitive as further investigations with alternative metal systems are required to support the finding that a high UPD metal monolayer coverage cannot be attained. Further, it was strongly indicated that oxidation of hydrogen-terminated BDD films must be avoided and minimised to increase the likelihood of observing UPD.

### **3.2.2 Oxygen-terminated Diamond Films**

Cu UPD onto an oxygen-terminated BDD film (sample B) was investigated in the same solutions as the hydrogen-terminated BDD films - 0.1 M H<sub>2</sub>SO<sub>4</sub> + 1 mM CuSO<sub>4</sub>, 2.5 mM CuSO<sub>4</sub> and 2.5 mM CuSO<sub>4</sub> + 0.5 mM KCl. The CVs for each of these solutions exhibited no signs of Cu UPD, only a bulk stripping peak at 0.04 V (Figure 21). This illustrated the highly sensitive surface nature of the UPD process and demonstrated that the oxygen termination inhibited Cu UPD.

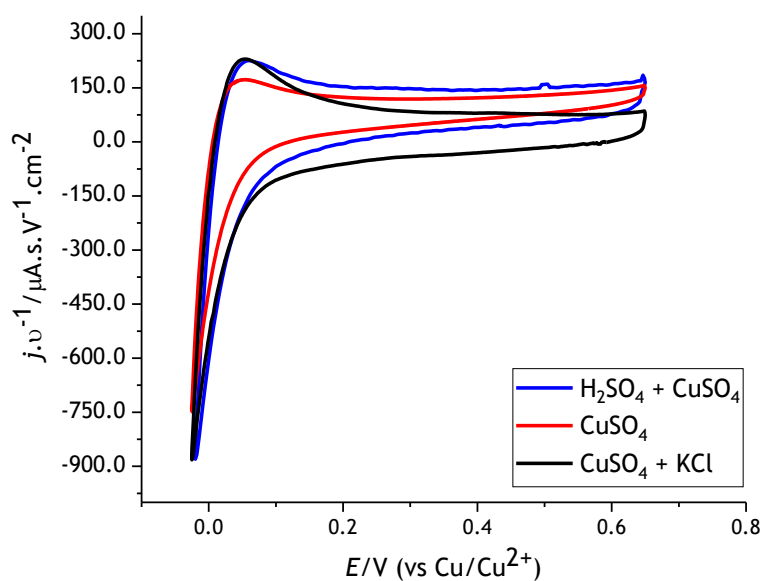


Figure 21: Cyclic voltammograms with sample B as the working electrode in 0.1 M H<sub>2</sub>SO<sub>4</sub> + 1 mM CuSO<sub>4</sub>, 2.5 mM CuSO<sub>4</sub> and 2.5 mM CuSO<sub>4</sub> + 0.5 mM KCl solutions - scan rate 20 mV s<sup>-1</sup>.

Oxygen plasma termination and ozone exposure were the two oxygen termination procedures used. These treatments terminate the BDD film surfaces with different ratios of ether- and carbonyl-bonded oxygens [96]. The different types of oxygen terminations did not appear to affect the Cu UPD observed because all the results were consistent, showing no signs of Cu UPD.

Oxygen-terminated BDD surfaces have been suggested to provide anchor points for Cu electrodeposition [97]. However, the results obtained did not confirm this. Instead, the oxygen termination was determined to inhibit the Cu UPD. The inhibition of Cu UPD was attributed to the large work function and low surface conductivity of the oxygen-terminated film relative to the hydrogen-terminated BDD films. The greater work function would have decreased the thermodynamic favourability of forming a Cu ad-layer, while the reduced surface conductivity would have decreased the ability for the electrode to interact with the Cu<sup>2+</sup> ions in solution [94]. Consequently, these properties would have

decreased the favourability of the electron transfer process from the BDD film to the  $\text{Cu}^{2+}$  ions, resulting in the inhibition of Cu UPD on the oxygen-terminated BDD film.

Thus, the UPD of Li and other metals onto oxygen-terminated BDD films to produce a diamond emitter with a metal oxide monolayer terminated surface appears unattainable. However, investigations into the electrochemical deposition of Li and other metals onto oxygen-terminated BDD films remain worthwhile to support the observations and conclusions arising from the inhibition of Cu UPD. As Li has a high affinity for the oxygen-terminated BDD surface, Li UPD onto an oxygen-terminated BDD film may occur more favourably than Cu UPD and overcome the energetic barrier proposed to inhibit Cu UPD.

The absence of Cu UPD on oxygen-terminated BDD films supported the conclusion that oxidation of the hydrogen-terminated BDD films would have reduced or inhibited Cu UPD over time. Therefore, no oxidation of a hydrogen-terminated BDD film surface is required to obtain the maximum UPD coverage.

### **3.3 Surface-Limited Redox Replacement (SLRR) Depositions**

SLRR depositions were used to replace Cu ad-layers on hydrogen-terminated BDD films with Pt in 0.5 mM  $\text{K}_2\text{PtCl}_4$  + 0.1 M  $\text{HClO}_4$ . These films were terminated 24 h prior to experimentation to minimise the oxidation of the electrode surface. CVs were run in the 2.5 mM  $\text{CuSO}_4$  solution on the Pt covered BDD films produced after the replacement of the Cu deposits. This was undertaken to identify changes in the CVs that corresponded to Cu deposition onto the Pt that covered the surface of the BDD film.

The CV in the 2.5 mM  $\text{CuSO}_4$  solution after the SLRR deposition of Pt with the Cu UPD on sample A did not show a distinctive change in the CV that would have indicated Cu deposition onto Pt (Figure 22). Subsequently, the CV did not signify that Pt covered the BDD film. This suggested that the SLRR deposition was either not successful or only

produced a small quantity of Pt on the surface of the BDD film. Thus, the Cu deposition peaks on Pt were not identifiable.

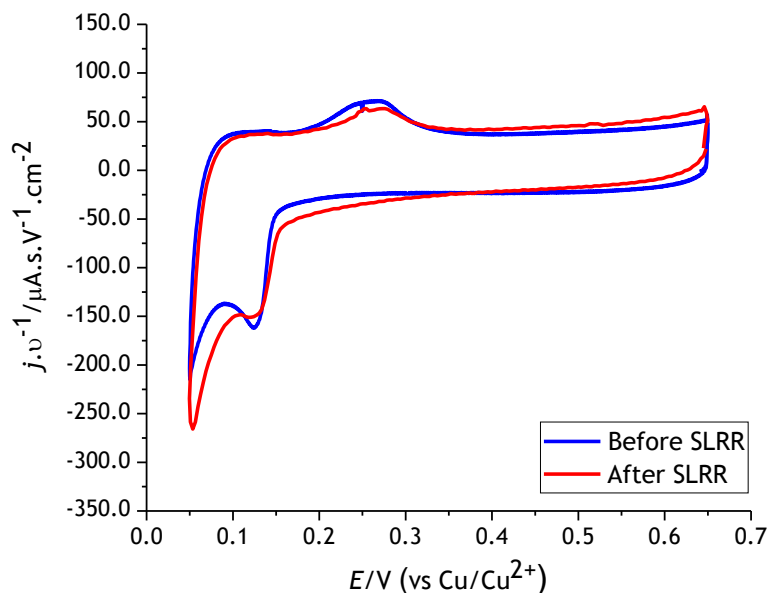


Figure 22: Cyclic voltammograms with a hydrogen-terminated sample A as the working electrode in a 2.5 mM  $CuSO_4$  solution before and after a SLRR deposition in 0.5 mM  $K_2PtCl_4$  + 0.1 M  $HClO_4$  - scan rate  $20 \text{ mV s}^{-1}$ .

The Cu UPD ad-layer was shown to achieve a ~2 % monolayer coverage rather than the ideal epitaxial monolayer. Therefore, even if the Cu deposit had been fully replaced with Pt, only a very small quantity of Pt would have been deposited onto the surface of the BDD film. Consequently, the absence of new peaks in the CV after the SLRR deposition was accounted for as a result of a very small quantity of Pt covering the surface of the electrode.

XPS analysis of the Pt-covered HFCVD BDD film confirmed a small quantity of Pt was present on the diamond film (Figure 23). The Pt 4f (5/2) and 4f (7/2) peaks at 76 and 73 eV, respectively, had a 0.05 % atomic percent relative to the C peak, while no peaks corresponding to Cu were evident (Figure 31) [95]. This proved that a SLRR deposition was able to replace the Cu UPD layer with Pt on a BDD film surface. However, this procedure

only achieved a small quantity of Pt on the electrode surface. The quantity of Pt deposited via the SLRR deposition was not close to the ideal epitaxial monolayer that could be achieved if a full Cu UPD monolayer deposit was attained. Nevertheless, this established that the SLRR procedure could be applied to BDD electrodes. Thus, if an epitaxial monolayer of a less noble metal can be underpotentially deposited, a SLRR deposition can be utilised to deposit a more noble catalytic metal onto a BDD with atomic scale precision for use in electrocatalysis.

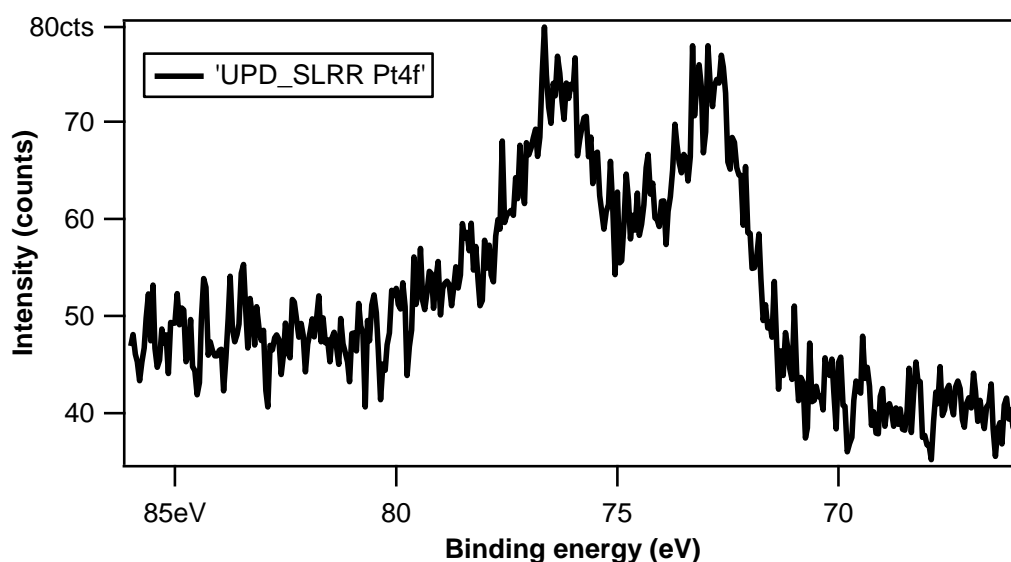


Figure 23: XPS spectrum of the Pt 4f peaks of the Pt ad-layer on sample A after the SLRR deposition of Pt with Cu UPD.

The SLRR procedure was modified to deposit a Cu layer, which was equivalent to a monolayer, at an overpotential. The modified procedure was undertaken to demonstrate the idea that SLRR depositions could be applied to BDD films provided that an increased UPD ad-layer coverage could be achieved. The charge of the Cu deposited was equivalent to the charge expected to form a monolayer to follow a SLRR based concept where a

controlled amount of metal deposited is replaced with a more noble metal on the surface of a substrate.

The quantity of Cu deposited to produce a layer equivalent to a monolayer was calculated from the considerations that the Cu lattice has a face-centred cubic crystal structure and the ad-layer had a (111) close-packed arrangement on a flat substrate. These considerations enabled the determination of the nearest neighbour distance between atoms, 2.6 Å, and subsequently the area of the unit cell from the lattice spacing, 3.6 Å [98]. From Equation 7 the area of the unit cell ( $A_0$ ) was used to determine the number of atoms per unit area ( $N$ ).

$$N = \frac{1}{A_0} \quad (7)$$

The number of atoms per unit area ( $N$ ) and elementary charge ( $e$ ) were used to calculate the charge transferred per unit area ( $Q$ ) that would correspond to the deposition of Cu equivalent to a monolayer (Equation 8).

$$Q = 2eN \quad (8)$$

A charge per unit area of 540  $\mu\text{C cm}^{-2}$  was calculated to deposit an amount of Cu equivalent to the amount ideally achieved by UPD. Therefore, 300  $\mu\text{C}$  of Cu was deposited onto 0.5  $\text{cm}^2$  of the electrochemical grade BDD film at a low overpotential. This quantity of charge transferred was determined to be a reasonable estimate for the sample because it accounted for the surface roughness and imperfections with a ~10 % overestimate of the charge. The overpotentially deposited Cu was assumed to cover the surface, however not uniformly.

The CVs in the 2.5 mM  $\text{CuSO}_4$  solution with the electrochemical grade BDD film before and after the modified SLRR deposition displayed significant differences. New peaks at 0.15 V and 0.40 V signified that Cu deposited onto the Pt that was on the surface of the BDD film

(Figure 24). The new peaks were smooth and covered a wide potential range, which is comparable to the CV of Cu UPD onto a polycrystalline Pt surface [99]. Therefore, these new peaks indicated that Pt was on the surface of the BDD. The current density after the SLRR deposition was also significantly greater than in the CV before the SLRR deposition. The greater current demonstrated a larger activated area than prior to the SLRR deposition, which is assumed to result from Pt covering the surface of the BDD film.

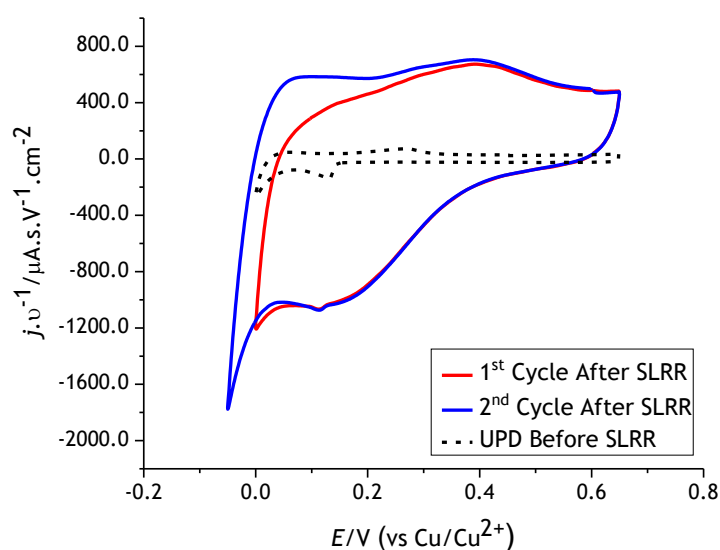


Figure 24: Cyclic voltammograms with a hydrogen-terminated electrochemical grade BDD film as the working electrode in a 2.5 mM  $\text{CuSO}_4$  solution before and after a modified SLRR deposition in 0.5 mM  $\text{K}_2\text{PtCl}_4$  + 0.1 M  $\text{HClO}_4$  - scan rate  $20 \text{ mV s}^{-1}$ .

The distinct changes in the CV are strong evidence that the modified SLRR deposition was successful and hence the electrochemical grade BDD film was covered in Pt. However, as the Cu was initially overpotentially deposited, an epitaxial monolayer was not formed, and subsequent characterisation of the structure was required. SEM showed numerous clusters present on the surface of the electrochemical grade BDD film (Figure 25). These small clusters are apparent on the surface after the SLRR deposition but not prior to the

electrochemical experiments (Figure 14). Thus, these clusters were formed from the SLRR deposition and likely corresponded to clusters of Pt on the surface.

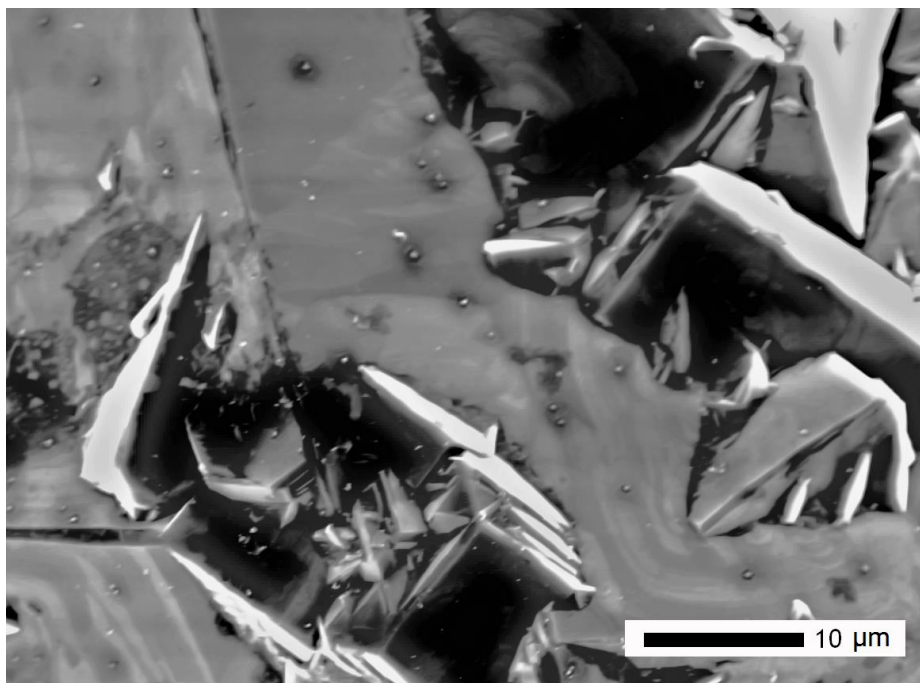


Figure 25: SEM image of the roughened side of the electrochemical grade boron-doped diamond film covered in small clusters of Pt (visible as small spots on the diamond surface) after the modified SLRR deposition.

XPS analysis clearly identified Pt 4f peaks (Figures 26 and 32). These Pt 4f peaks further established that the clusters observed in SEM corresponded to Pt. The Pt 4f peaks were about 7.5 times greater in intensity than the Pt 4f peaks identified after the Cu UPD ad-layer was used in the SLRR deposition (Figure 23). The increased quantity of Pt deposited supported the idea that a SLRR deposition could be applied to a BDD film. In the modified SLRR procedure investigated, clusters of Pt were formed as opposed to the ideal epitaxial monolayer. However, if an epitaxial metal monolayer can be deposited on a BDD film, this research suggests that a SLRR process could be applied to deposit an electrocatalyst monolayer onto a BDD electrode with high sensitivity.

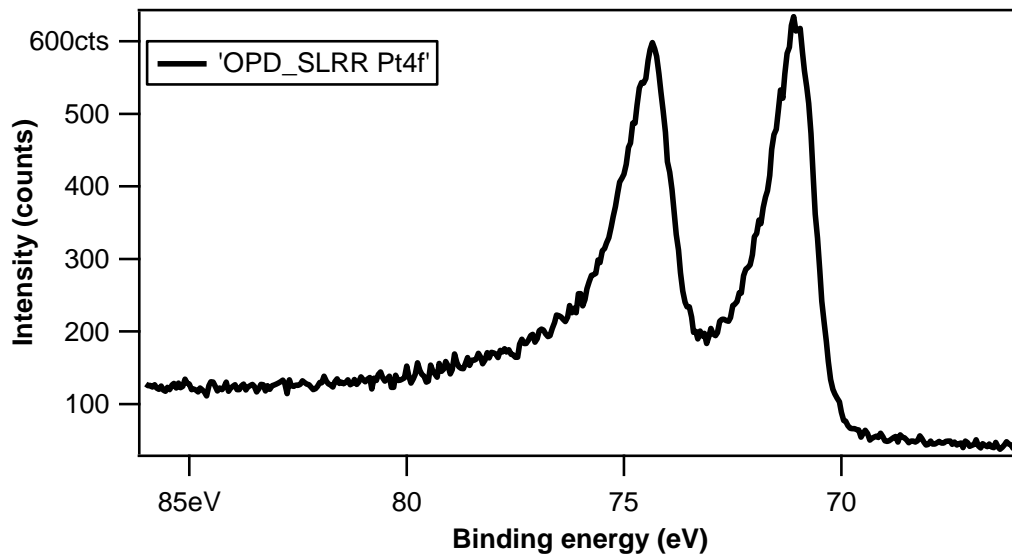


Figure 26: XPS spectrum of the Pt 4f peaks of the Pt ad-layer on the electrochemical grade boron-doped diamond film after the modified SLRR deposition of Pt with Cu.

XPS detected small quantities of Cu with peaks at 952 and 933 eV (Figure 27). The Cu peaks had 0.4 % atomic percent relative to the C peak. This indicated that the Cu was not completely replaced with Pt in the SLRR deposition. The small quantity of Cu remaining on the BDD film most likely related to the partial alloying of Cu with the Pt deposit.

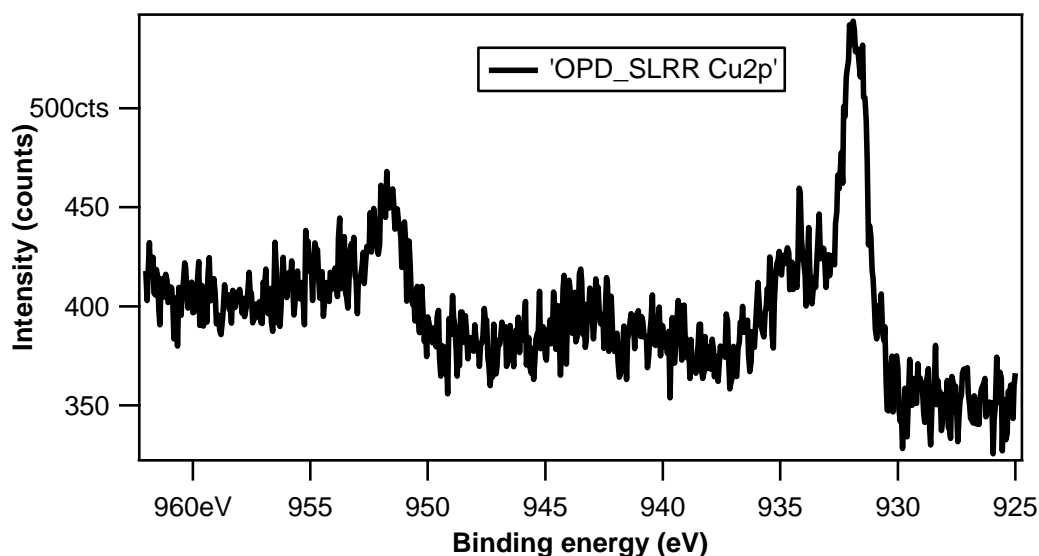


Figure 27: XPS spectrum of the Cu 2p peaks present in the Pt ad-layer on the electrochemical grade boron-doped diamond film after the modified SLRR deposition of Pt with Cu.

The finding that Pt was deposited onto the BDD film in the SLRR deposition demonstrated that an electrocatalyst could be deposited onto a BDD via this electrochemical deposition technique. However, the ability of this technique to deposit a monolayer of a catalytic metal onto the surface of a BDD film relies on achieving a homogenous high coverage ad-layer of a metal that is less noble than the noble metal being deposited. This ideal UPD metal monolayer coverage could not be attained with Cu on a BDD film. Nevertheless, further investigations into alternative metals or deposition methods may facilitate the ability to produce an epitaxial monolayer on a hydrogen-terminated BDD film. If achieved this would enable the use of SLRR depositions to deposit catalytic metals on BDD films with atomic scale precision for use in electrocatalysis.

## Chapter 4: Conclusions

Cu UPD was achieved on hydrogen-terminated BDD films in solutions at various pH values. In a 2.5 mM CuSO<sub>4</sub> electrolyte solution, Cu UPD was displayed at ~2 % monolayer coverage. Thus, it was suggested that the Cu deposited in the favourable sites located at the grain boundaries of the BDD films. Cu UPD was observed at a lower extent in a 0.1 M H<sub>2</sub>SO<sub>4</sub> + 1 mM CuSO<sub>4</sub> solution relative to a 2.5 mM CuSO<sub>4</sub> electrolyte solution. The greater quantity of Cu UPD exhibited in a 2.5 mM CuSO<sub>4</sub> solution correlated to the increased favourable Coulombic interaction between the BDD film surface and the Cu<sup>2+</sup> ions, as well as the better surface quality of the electrode. The presence of 0.5 mM KCl in the 2.5 mM CuSO<sub>4</sub> electrolyte resulted in a decrease in the Cu UPD observed. The corresponding decrease in UPD was suspected to partially result from additional interactions between Cl<sup>-</sup> ions and the BDD film, as well as Cl<sup>-</sup> ions complexing with the Cu<sup>2+</sup> ions. These additional interactions were assumed to have contributed to the decrease of Cu UPD. However, the poorer surface quality of the electrode used in the 0.1 M H<sub>2</sub>SO<sub>4</sub> + 1 mM CuSO<sub>4</sub> and 2.5 mM CuSO<sub>4</sub> + 0.5 mM KCl solutions was the main factor that caused to the reduction in UPD observed.

The surface quality of the BDD film was established to be a significant factor limiting the observed UPD. Oxidation at the grain boundaries of the hydrogen-terminated BDD electrodes, between the termination procedure and electrochemical deposition experiments, was concluded to inhibit Cu UPD. A cathodic activation process was required to modify the surface C-O functionalities into C-H functionalities. The activation process was essential for a Cu UPD peak to be displayed in the 0.1 M H<sub>2</sub>SO<sub>4</sub> + 1 mM CuSO<sub>4</sub> and 2.5 mM CuSO<sub>4</sub> + 0.5 mM KCl solutions. Small UPD peaks were observed after the activation process and consequently indicated that Cu was deposited onto the surface in minimal quantities. Thus, the time between the termination procedure and electrochemical investigations must be minimised to less than a few days to ensure that the surface quality of the hydrogen-terminated BDD electrode is sufficient to observe UPD.

Oxygen termination of BDD films inhibited Cu UPD. The oxygen-terminated surface inhibition of Cu UPD was associated with the large work function and low surface conductivity of the material relative to the hydrogen-terminated BDD films. These properties were determined to reduce the favourability of the electron transfer process to  $\text{Cu}^{2+}$  ions, subsequently preventing Cu UPD. Thus, using UPD to produce a metal-oxide-terminated surface that would be suitable for applications in thermionic emission devices consequently appears to be unfeasible. However, future investigations into metals with a high affinity to the oxygen-terminated diamond surface, such as Li, remain worthwhile to fully establish the feasibility of using UPD to produce a diamond emitter.

SLRR depositions were successfully applied to the BDD films, replacing the Cu ad-layer with Pt in 0.5 mM  $\text{K}_2\text{PtCl}_4$  + 0.1 M  $\text{HClO}_4$ . The capability to deposit catalytic metals sensitively onto a BDD surface facilitates the synthesis of BDD catalyst supports via UPD. However, as Cu UPD was unable to attain a metal ad-layer of considerable coverage on the BDD films, the Pt deposited by the SLRR deposition had an insufficient coverage for electrocatalysis applications. This inability to achieve an ideal epitaxial Cu monolayer demonstrated that UPD is currently unable to produce the metal terminations required for extensive electrocatalysis and thermionic emission applications. Nevertheless, provided an epitaxial monolayer of a metal less noble than the desired catalytic metal could be achieved, a SLRR deposition would be suitable to deposit a monolayer of a catalytic metal onto a BDD film.

## Chapter 5: Future Work

Significant optimisation of the UPD metal systems is required to make reproducible metal monolayers on BDD films attainable. Investigating alternative metals to electrodeposit, such as Ag, Pt and Au, onto the surface of the BDD films would be a worthwhile investigation to determine whether alternative systems could achieve the desired monolayer coverage. These systems should be investigated at a range of pH values to progress the understanding identified in this research that more favourable Coulombic interactions can encourage UPD to occur.

Terminating a diamond surface with Li via electrochemical deposition techniques remains an interesting alternative method to produce a diamond emitter. Li UPD onto the diamond surface using  $\text{LiClO}_4$  in acetonitrile solution was unable to be investigated in this project and subsequently is ideal for future investigations. Even though UPD on oxygen-terminated BDD films was deemed unfeasible for Cu, deposits of Li have been shown to have a strong adhesion to the surface of an oxygen-terminated diamond film. Thus, characterising the surface coverage and structural arrangement of Li on BDD deposited via UPD and overpotential deposition would clarify whether the possibility of producing a diamond emitter from an electrochemical technique is a realisable possibility. This experiment would require stringent precautionary measures to ensure the absence of moisture from the solution and environment, as moisture inhibits Li deposition.

Provided the attainment of relatively inexpensive single-crystal BDD films, electrochemical depositions of metals onto single-crystal BDD films would be an ideal future investigation to extend on this research, which focused on polycrystalline BDD films. This would progress the current understanding of the electrochemical deposition of metals onto BDD films and aid our ability to form a metal monolayer.

## Chapter 6: References

- [1] M. Paunovic, M. Schlesinger, *Fundamentals of Electrochemical Deposition*, John Wiley and Sons, New Jersey, 2006.
- [2] S. Hermans, T.V. de Bocarme, *Atomically-Precise Methods for Synthesis of Solid Catalysts*, Royal Society of Chemistry Publishing, Cambridge, 2014.
- [3] G.E. Rhead, *Contemporary Physics*, 1983, **24**, 6, 535-559.
- [4] S. Szabó, *International Reviews in Physical Chemistry*, 1991, **10**, 2, 207-248.
- [5] O.A. Oviedo, L. Reinaudi, S.G. García, E.P.M. Leiva, *Underpotential Deposition: From Fundamentals and Theory to Applications at the Nanoscale*, Springer, Berlin, 2015.
- [6] E.P.M Leiva, *Electrochimica Acta*, 1996, **14**, 2185-2206.
- [7] F. Scholz, E.P.M. Leiva, *ChemElectroChem*, 2017, **4**,1-7.
- [8] D.M. Kolb, M. Przasnyski, H. Gerischer, *Electroanalytical Chemistry and Interfacial Electrochemistry*, 1974, **54**, 25-38.
- [9] E. Herrero, L.J. Buller, H.D. Abruna, *Chem. Rev.*, 2001, **101**, 1897-1930.
- [10] J.W. Schultze, D. Dickertmann, *Surface Science*, 1976, **54**, 489-505.
- [11] J. Nutariya, M. Fayette, N. Dimitrov, N. Vasiljevic, *Electrochimica Acta*, 2013, **112**, 813-823.
- [12] R.R. Adzic, J. Zhang, K. Sasaki, M.B. Vukmirovic, M. Shao, J.X. Wang, A.U. Nilekar, M. Mavrikakis, J.A. Valerio, F. Uribe, *Topics in Catalysis*, 2007, **46**, 249-262.
- [13] S. Ambrozik, B. Rawlings, N. Vasiljevic, N. Dimitrov, *Electrochemistry Communications*, 2014, **44**, 19-22.
- [14] M. Muthuvel, J.L. Stickney, *Langmuir*, 2006, **22**, 5504-5508.
- [15] G. Pezzatini, S. Caporali, M. Innocenti, M.L. Foresti, *Journal of Electroanalytical Chemistry*, 1999, **475**, 164-170.
- [16] J.O'M. Bockris, R.E. White, B.E. Conway, *Modern Aspects of Electrochemistry*, Volume 31, Springer Science & Business Media, Berlin, 2006.

- [17] S. Swathirajan, S. Bruckenstein, *Electrochimica Acta*, 1983, **28**, 865-877.
- [18] J.O'M. Bockris, S.U.M. Khan, *Surface Electrochemistry: A Molecular Level Approach*, Springer Science & Business Media, Berlin, 1993.
- [19] C.G. Sanchez, E.P.M. Leiva, J. Kohanoff, *Langmuir*, 2001, **17**, 2219-2227.
- [20] G. Herzog, D.W.M. Arrigan, *Trends in Analytical Chemistry*, 2005, **24**, 3, 208-217.
- [21] W. Schmickler, *Chemical Physics*, 1990, **141**, 95-104.
- [22] I. Tiginyanu, P. Topala, V. Ursaki, *Nanostructures and Thin Films for Multifunctional Applications: Technology, Properties and Devices*, Springer, Berlin, 2016.
- [23] V. Sudha, M. V. Sangaranarayanan, *J. Phys. Chem. B*, 2002, **106**, 2699-2707.
- [24] W. Plieth, *Electrochemistry for Materials Science*, Elsevier, Amsterdam, 2008.
- [25] M.L. Foresti, M. Innocenti, F. Forni, R. Guidelli, *Langmuir*, 1998, **14**, 7008-7016.
- [26] N. Dimitrov, R. Vasilic, N. Vasiljevic, *Electrochemical and Solid-State Letters*, 2007, **10**, 7, D79-D83.
- [27] E.B. Budevski, G.T. Staikov, W.J. Lorenz, *Electrochemical Phase Formation and Growth: An Introduction to the Initial Stages of Metal Deposition*, John Wiley and Sons, New Jersey, 2008.
- [28] S. Swathirajan, S. Bruckenstein, *J. Electroanal. Chem.*, 1983, **146**, 137-155.
- [29] M. Paunovic, D. Scherson, *Proceedings of the Third Symposium on Electrochemically Deposited Thin Films*, The Electrochemical Society, New Jersey, 1997.
- [30] C. Silien, M. Buck, *J. Phys. Chem. C*, 2008, **112**, 3881-3890.
- [31] S. Garcia, D. Salinas, C. Mayer, E. Schmidt, G. Staikov, W.J. Lorenz, *Electrochimica Acta*, 1998, **43**, 19-20, 3007-3019.
- [32] C.R. Fuselier, J.C. Raich, N.S. Gillis, *Surf. Sci.*, 1980, **92**, 667-680.
- [33] D.M. Kolb, *Surface Science*, 2002, **500**, 722-740.

- [34] N. Vasiljevic, L.T. Viyannalage, N. Dimitrov, K. Sieradzki, *Journal of Electroanalytical Chemistry*, 2008, **613**, 118-124.
- [35] M. Nishizawa, T. Sunagawa, H. Yoneyama, *Langmuir*, 1997, **13**, 5215-5217.
- [36] C.H. Chen, S.M. Vesecky, A.A. Gewirth, *J. Am. Chem. Soc.*, 1992, **114**, 451-458.
- [37] J.G. Xu, X.W. Wang, *Surface Science*, 1998, **408**, 317-325.
- [38] P.W. May, *Phil. Trans. R. Soc. Lond. A*, 2000, **358**, 473-495.
- [39] H.J. Fecht, K. Brühne, *Carbon-based Nanomaterials and Hybrids: Synthesis, Properties, and Commercial Applications*, CRC Press, Florida, 2016.
- [40] U.S. Geological Survey, *Minerals Yearbook, 2008, V. 1, Metals and Minerals*, Government Printing Office, Washington, 2011.
- [41] K.E. Spear, J.P. Dismukes, *Synthetic Diamond: Emerging CVD Science and Technology*, John Wiley and Sons, New Jersey, 1994.
- [42] Società italiana di fisica, *The Physics of Diamond*, IOS Press, Amsterdam, 1997.
- [43] T. Moeller, *Chemistry: With Inorganic Qualitative Analysis*, Elsevier, Amsterdam, 2012.
- [44] G.L. Hornyak, H.F. Tibbals, J. Dutta, J.J. Moore, *Introduction to Nanoscience and Nanotechnology*, CRC Press, Florida, 2008.
- [45] W. Ahmed, M.J. Jackson, *Surgical Tools and Medical Devices*, Springer, New York, 2016.
- [46] Koji Kobashi, Kozo Nishimura, Yoshio Kawate, Takefumi Horiuchi, *Phys. Rev. B*, 1998, **38**, 4067.
- [47] M. Kamo, Y. Sato, S. Matsumoto, N. Setaka, *Journal of Crystal Growth*, 1983, **62**, 3, 642-644.
- [48] S. Matsumoto, Y. Sato, M. Kamo, N Setaka, *Japanese Journal of Applied Physics*, 1982, **21**, 4, 183-185.
- [49] J.C. Angus, *Diamond & Related Materials*, 2014, **49**, 77-86.
- [50] P.W. May, *Endeavour*, 1995, **19**, 3, 101-106.

- [51] S.T. Lee, H.Y. Peng, X.T. Zhou, N. Wang, C.S. Lee, I. Bello, Y. Lifshitz, *Science*, 2000, **287**, 5450, 104-106.
- [52] K. Nassau, *Color for Science, Art and Technology*, Elsevier, Amsterdam, 1997.
- [53] R.S. Sussmann, *CVD Diamond for Electronic Devices and Sensors*, John Wiley & Sons, New Jersey, 2009.
- [54] V. Seshan, D. Ullien, A. Castellanos-Gomez, S. Sachdeva, D.H.K. Murthy, T.J. Savenije, H.A. Ahmad, T.S. Nunnery, S.D. Janssens, K. Haenen, M. Nesládek, H.S.J. van der Zant, E.J.R. Sudhölter, L.C.P.M. de Smet, *The Journal of Chemical Physics*, 2013, **138**, 234707.
- [55] I.L. Krainsky, V.M. Asnin, *Appl. Phys. Lett.*, 1998, **72**, 2574.
- [56] S.J. Pearton, *GaN and Related Materials II*, CRC Press, Florida, 2000.
- [57] D. Takeuchi, C.E. Nebel, S. Yamasaki, *Journal of Applied Physics*, 2006, **99**, 086102.
- [58] H.D Andrade, M.Z. Othman, K.M. O'Donnell, J.H. Lay, P.W. May, N.A. Fox, *Int. J. Nanotechnol.*, 2014, **11**, 796-807.
- [59] F. Bouamrane, A. Tadjeddine, R. Tenne, J.E. Butler, R. Kalish, C. Levy-Clement, *J. Phys. Chem. B*, 1998, **102**, 134-140.
- [60] B. Duran, R.F. Brocenschi, M. France, J.J. Galligan, G.M. Swain, *Analyst.*, 2014, **139**, 3160-3166.
- [61] H.B. Suffredini, V.A. Pedrosa, L. Codognoto, S.A.S. Machado, R.C. Rocha-Filho, L.A. Avaca, *Electrochimica Acta*, 2004, **49**, 4021-4026.
- [62] E. Mahe, D. Devilliersa, Ch. Comninellis, *Electrochimica Acta*, 2005, **50**, 2263-2277.
- [63] W. Hongthani, N.A. Fox, D.J. Fermín, *Langmuir*, 2011, **27**, 5112-5118.
- [64] H. Aitchison, N. Meyerbroker, T.L Lee, J. Zegenhagen, T. Potter, H. Fruchtl, I. Cebulac, M. Buck, *Phys. Chem. Chem. Phys.*, 2017, **19**, 24146.
- [65] K.A.A. Khalid, T.J. Leong, K. Mohamed, *IEEE Transactions on Electron Devices*, 2016, **63**, 6, 2231-2241.

- [66] V.C. Wilson, *Journal of Applied Physics*, 1959, **30**, 475.
- [67] A. Fridman, *Plasma Chemistry*, Cambridge University Press, Cambridge 2008.
- [68] T. Ito, M.A. Cappelli, *Applied Physics Letters*, 2012, **101**, 213901.
- [69] L. Marton, C. Marton, *Advances in Electronics and Electron Physics, Volume 17*, Academic Press, Cambridge, 1963.
- [70] A. Fridman, *Plasma Chemistry*, Cambridge University Press, 2008.
- [71] K.Y. Cheong, *Two-Dimensional Nanostructures for Energy-Related Applications*, CRC Press, Florida, 2017.
- [72] W.F. Paxton, A. Steigerwald, M. Howell, N. Tolk, W.P. Kang, J.L. Davidson, *Applied Physics Letters*, 2012, **101**, 243509.
- [73] A.K. Tiwari, J.P. Goss, P.R. Briddon, A.B. Horsfall, N.G. Wright, R. Jones, M.J. Rayson, *EPL*, 2014, **108**, 46005.
- [74] P.K. Baumann, R.J. Nemanich, *Phys Rev B*, 1998, **58**, 3, 1643-1654.
- [75] K.M. O'Donnell, T.L. Martin, N.A. Fox, D. Cherns, *Phys. Rev. B*, 2010, **82**, 115303.
- [76] A. De Battisti, S. Ferro, M. Dal Colle, *J. Phys. Chem. B*, 2001, **105**, 9, 1679-1682.
- [77] A. Wieckowski, E.R. Savinova, C.G. Vayenas, *Catalysis and Electrocatalysis at Nanoparticle Surfaces*, CRC Press, Florida, 2003.
- [78] A.B. Couto, M.C.E. Ribeiro, F.L. Migliorini, N.G. Ferreira, M.R. Baldan, *Diamond & Related Materials*, 2013, **38**, 104-108
- [79] N. Yang J.S. Foord, X. Jiang, *Carbon*, 2016, **99**, 90-110.
- [80] G.R. Salazar-Banda, K.I.B. Eguiluz, L.A. Avaca, *Electrochemistry Communications*, 2007, **9**, 59-64.
- [81] C.K. Mavrokefalos, G.W. Nelson, C.G. Poll, R.G. Compton, J.S. Foord, *Phys. Status Solidi A*, 2015, **212**, 11, 2559-2567.
- [82] G. Siné, I. Duo, B. El Roustom, G. Fóti, Ch. Comninellis, *Journal of Applied Electrochemistry*, 2006, **36**, 847-862.
- [83] A.Y. Stakheev, L.M. Kustov, *Applied Catalysis A: General*, 1999, **188**, 3-35.

- [84] Element Six, <http://e6cvd.com/uk/application/electrochemistry/pe-10x10-mm-0-6-mm-thick.html>, (accessed April 2018).
- [85] D.S. Knight, W.B. White, *J. Mater. Res.*, 1989, **4**, 385-393.
- [86] S. Praver, R.J. Nemanich, *Phil. Trans. R. Soc. Lond. A*, 2004, **362**, 2537-2565.
- [87] P.W. May, W.J. Ludlow, M. Hannaway, P.J. Heard, J.A. Smith, K.N. Rosser, *Diamond & Related Materials*, 2008, **17**, 105-117.
- [88] M.A. Prelas, G. Popovici, L.K. Bigelow, *Handbook of Industrial Diamonds and Diamond Films*, CRC Press, Florida, 1997.
- [89] L.A. Hutton, J.G. Iacobini, E. Bitziou, R.B. Channon, M.E. Newton, J.V. Macpherson, *Anal. Chem.*, 2013, **85**, 7230-7240.
- [90] C.L. Scortichini, C.N. Reilley, *J. Electroanal. Chem.*, 1982, **139**, 247-264.
- [91] F. Rodriguez, D.L. Taylor, H.D. Abruna, *Electrochimica Acta*, 1993, **38**, 235-244.
- [92] C.L. Scortichini, C.N. Reilley, *J. Electroanal. Chem.*, 1982, **139**, 233-245.
- [93] F. Bouamrane, A. Tadjeddine, J.E. Butler, R. Tenne, C. Levy-Clement, *Journal of Electroanalytical Chemistry*, 1996, **405**, 95-99.
- [94] C. Nebel, J. Ristein, *Thin-Film Diamond I*, Academic Press, Cambridge, 2003.
- [95] NIST X-ray Photoelectron Spectroscopy Database, <https://srdata.nist.gov/xps/Default.aspx>, (accessed March 2018).
- [96] J.V. Macpherson, *Phys. Chem. Chem. Phys.*, 2015, **17**, 2935-2949.
- [97] A.B. Couto, L.C.D. Santos, J.T. Matsushima, M.R. Baldan, N.G. Ferreira, *Applied Surface Science*, 2011, **257**, 10141-10146.
- [98] S.M. Foiles, M.I. Baskes, M.S. Daw, *Phys. Rev. B*, 1986, **33**, 7983.
- [99] D. Simkunaite, I. Valsiunas, A. Steponavicius, *Russian Journal of Applied Chemistry*, 2009, **82**, 2139-2145.
- [100] C.G. Zoski, *Handbook of Electrochemistry*, Elsevier, New York, 2007.

## Chapter 7: Appendix

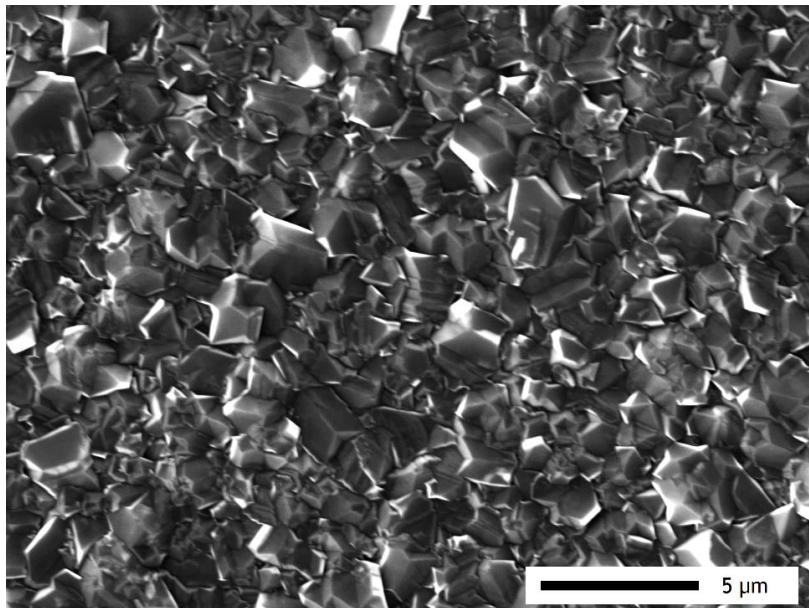


Figure 28: SEM image of a boron-doped diamond film, denoted sample B, synthesised in a hot filament CVD reactor.

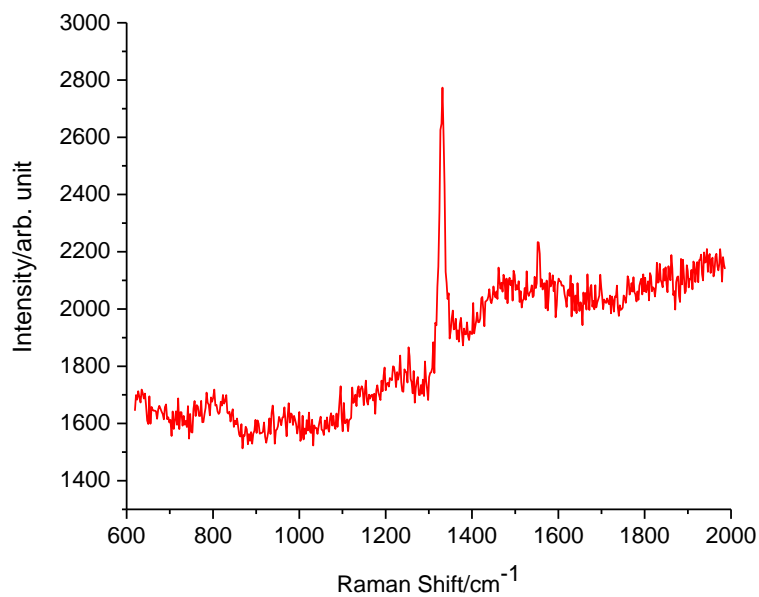


Figure 29: Raman spectrum of a boron-doped diamond film synthesised in a hot filament CVD, denoted sample A, using a green 514 nm laser.

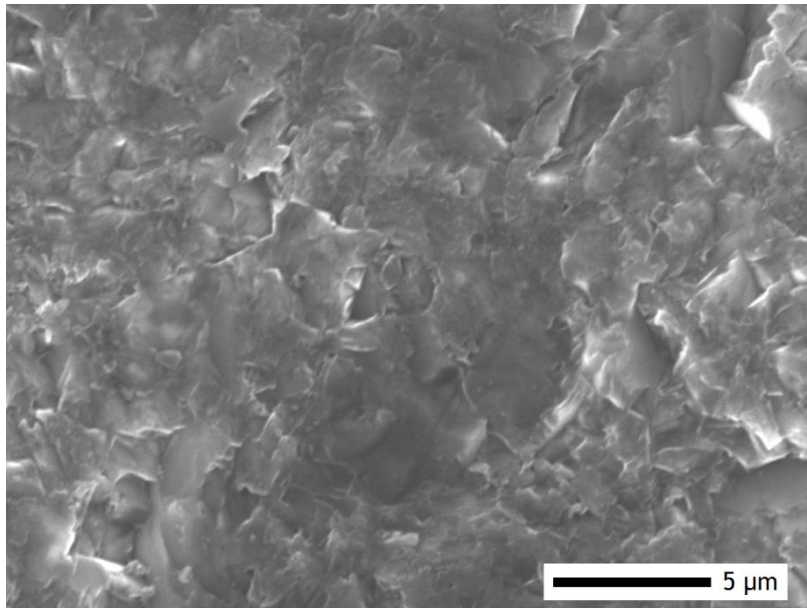


Figure 30: SEM image of the smooth side of the electrochemical grade boron-doped diamond film purchased from Element Six.

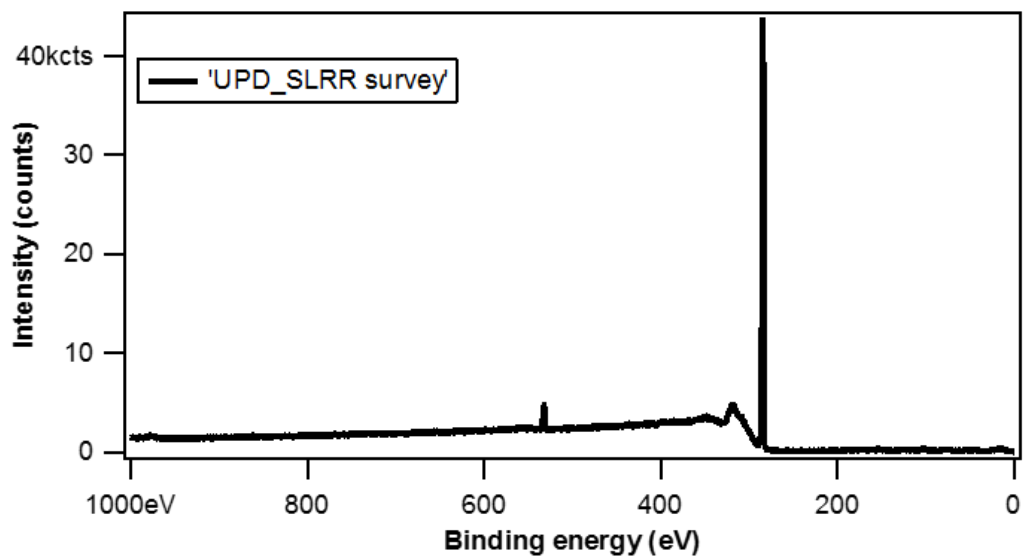


Figure 31: XPS survey scan of the Pt covered sample A after the SLRR deposition of Pt with Cu UPD from 0 to 1000 eV.

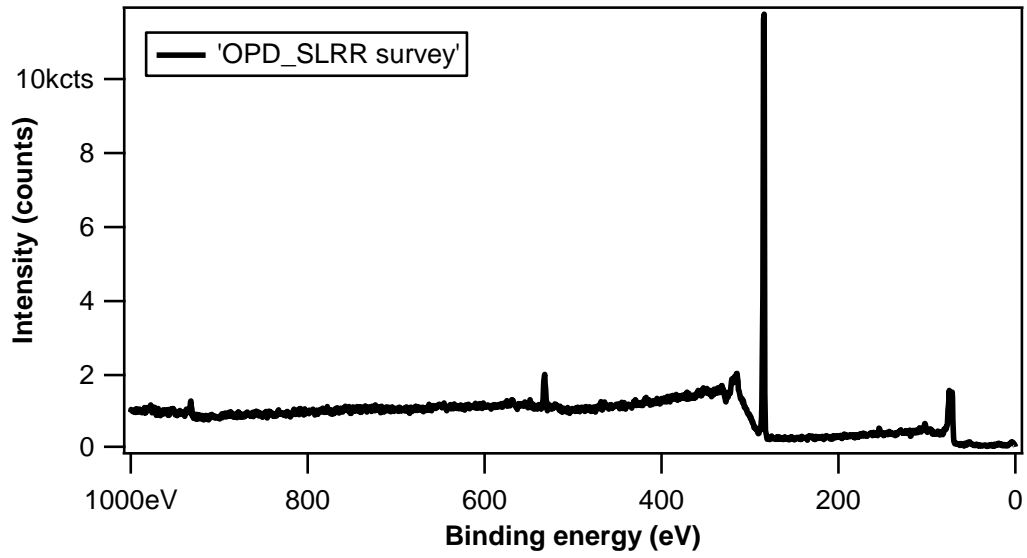


Figure 32: XPS survey scan of the Pt covered electrochemical grade BDD film after the modified SLRR deposition of Pt with Cu from 0 to 1000 eV.